

# **Ligand Binding Properties of Giardia Flavohemoglobin**

A thesis submitted to the Committee of Graduate Studies in partial fulfillment of the requirements for the degree of Master of Science in the Faculty of Arts and Science

Trent University  
Peterborough, Ontario, Canada

© Copyright by Novin Nezamololama 2019  
Environmental and Life Sciences M.Sc. Graduate Program  
September 2019

## ABSTRACT

### Ligand Binding Properties of *Giardia* Flavohemoglobin Novin Nezamololama

The parasitic protist *Giardia intestinalis* possesses flavohemoglobin (gFIHb), an enzyme that detoxifies nitric oxide to the less harmful nitrate, and is a potential target for anti-giardial drugs that act as ligands to the iron of its heme cofactor. In this work, the binding constants  $K_D$  of gFIHb, three active-site variants (Q54L, L58A, Y30F) and the *E. coli* flavohemoglobin (Hmp) towards cyanide, azide and several substituted imidazoles were measured by optical titration. Certain cases such as gFIHb and Hmp were studied further by isothermal titration calorimetry. Binding constants for cyanide and the imidazoles ranged from 2 to 100  $\mu\text{M}$ , with the highest affinities observed with miconazole, a bulky substituted imidazole. Azide was a poor ligand, with binding constants between 0.48 and 26 mM. Among gFIHb and its mutants, L58A tended to have the highest ligand affinities, as mutation of the distal leucine to a less bulky distal alanine residue facilitates the access of the exogenous ligand to the heme iron. In contrast, the Q54L and Y30F variants had binding affinities that in most cases were similar to wild type, which suggests that the inability of their side chains to form hydrogen bonds to these ligands is not a significant factor in binding of imidazole ligands to the enzyme. Comparative results for Hmp and gFIHb ligand binding affinities revealed slight differences which might be explained by the presence of different residues in their active sites apart from their conserved residues.

**Keywords:** flavohemoglobin, *Giardia intestinalis*, gFIHb, ligand binding, substituted-imidazole ligands, nitrosative stress, heme protein, nitric oxide detoxification, Hmp, UV-Visible spectroscopy, ITC

## ACKNOWLEDGEMENTS

First of all, I would like to thank Dr. Steven Rafferty for his support. He is not only a great supervisor but also a wise, caring and kind person. Thank you for enlightening me and making this journey filled with good memories. I will never forget how you answered my countless questions with passion and how you would always come to the lab to make sure I had a good understanding for what you explained to me. I could not have asked for a better supervisor. I would also like to thank Dr. Janet Yee for all her help and for letting me use her lab during the course of my masters.

I would also like to thank my committee members, Dr. Andrew Vreugdenhil and Dr. Holly Bates. I appreciate all your support and advice. To Linda Cardwell of the ENLS graduate program, you are an amazing person with a big heart, and you are great at what you are doing. To Guy Guillemette of the University of Waterloo, thank you for letting me stay with you and your family while I was doing ITC experiments. And to Harmeem Deol of Waterloo, thank you for teaching me how to use ITC and for helping me troubleshoot when things were not working as expected.

I would also like to express my gratitude to the present and past members of Yee/ Rafferty lab including Erika Crowley, Eliza McColl, Kaitlyn Mowat, William Batoff, Guillem Dayer, Brian Lukaszewicz, Bayan Sajer, Zakhar Krekhno, Jessica Chorolovski, Rodion Gordzevich, Angus Sullivan and Markus King. To Erika Crowley, thanks for being a great lab mate and for always coming up with great lab ideas. To Eliza McColl, thank you for passing on your knowledge about Giardia to me. You were the first person I came to talk to after considering doing a masters in this field and I am always grateful for taking your advice.

Last but not least, I would like to say thank you to my family and friends without whom this would be impossible for me to accomplish. Words cannot describe how grateful I am to each one of you.

## TABLE OF CONTENTS

ABSTRACT.....	ii
ACKNOWLEDGEMENTS.....	iii
LIST OF FIGURES .....	vi
LIST OF TABLES.....	vii
LIST OF ABBREVIATIONS AND SYMBOLS.....	viii
<b>1. INTRODUCTION .....</b>	<b>1</b>
1.1 Giardia intestinalis .....	1
1.2 Host-generated Nitric Oxide (NO) and its Effects on Giardia.....	3
1.3 Flavohemoglobin Function, Mechanism, and Structure.....	4
1.3.1 Function and Structure.....	4
1.3.2 Active Site Structure of Flavohemoglobin .....	6
1.3.3 Nitric Oxide Dioxygenase Activity of Flavohemoglobins .....	10
1.4 Characteristics of Giardia Flavohemoglobin .....	12
1.5 Isothermal Titration Calorimetry (ITC).....	17
1.6 Thesis Aims .....	18
<b>2. PROCEDURES .....</b>	<b>21</b>
2.1 Protein Expression and Purification... ..	21
2.1.1 Protein Expression... ..	21
2.1.2 Protein Purification .....	22
2.2 Assessment of Lipid Binding to Flavohemoglobins.....	26
2.3 Optical Titration of Flavohemoglobin with Exogenous Ligands .....	27
2.4 Isothermal Titration Calorimetry (ITC) of Ligand Binding to Flavohemoglobins .....	29

3. RESULTS AND DISCUSSION.....	31
3.1 Protein Expression and Purification .....	31
3.2 UV-Visible Spectroscopy .....	32
3.3 Optical Titrations of gFlHb and Variants .....	37
3.4 Isothermal Titration Calorimetry .....	42
3.5 Future Directions .....	47
3.6 Conclusions.....	48
REFERENCES .....	49

## LIST OF FIGURES

<b>Figure 1:</b> Homology model of gFlHb based on the structure of <i>E. coli</i> Hmp.....	5
<b>Figure 2:</b> Heme cofactor of flavohemoglobins .....	7
<b>Figure 3:</b> Active site residues in flavohemoglobins.....	8
<b>Figure 4:</b> Catalytic cycle for NO-dioxygenase activity of flavohemoglobin.....	11
<b>Figure 5:</b> Heme active site and miconazole binding to the heme iron of flavohemoglobins.....	14
<b>Figure 6:</b> Spectroscopic changes in flavohemoglobin on binding of a ligand.....	16
<b>Figure 7:</b> One-site model binding isotherm and thermogram obtained by ITC.....	18
<b>Figure 8:</b> Active site residues of gFlHb and Hmp .....	20
<b>Figure 9:</b> Sequence alignment of gFlHb and Hmp .....	20
<b>Figure 10:</b> SDS-PAGE gel indicating the purified gFlHb, its distal mutants and Hmp... ..	25
<b>Figure 11:</b> Overlaid UV-Visible spectra for WT gFlHb, its variants and Hmp.....	33
<b>Figure 12:</b> Overlaid UV-Visible spectra for Hmp before and after phospholipid removal .....	35
<b>Figure 13:</b> Detection of phospholipids by using TLC plates .....	36
<b>Figure 14:</b> Optical titration example with fitted curve.....	37
<b>Figure 15:</b> Movement of E-helix upon binding of econazole in Yhb... ..	40
<b>Figure 16:</b> Raw thermograms and analyzed ITC data for gFlHb and Hmp.....	42

**LIST OF TABLES**

<b>Table 1:</b> Properties of ligands used in this work.....	28
<b>Table 2:</b> Protein expression yield for gFlHb and Hmp... ..	31
<b>Table 3:</b> Dissociation constants of heme-binding ligands for gFlHb and its distal mutants determined by optical titrations .....	39
<b>Table 4:</b> Dissociation constants of heme-binding ligands for gFlHb and Hmp determined by optical titration.....	41
<b>Table 5:</b> Distal site residue differences between gFlHb and Hmp.....	41
<b>Table 6:</b> Dissociation constants from ITC for ligand binding to flavohemoglobins.....	43
<b>Table 7:</b> Thermodynamic parameters from ITC for ligand binding to flavohemoglobins .....	43

**LIST OF ABBREVIATIONS AND SYMBOLS**

<b>ADI</b>	Arginine Deiminase
<b>ATP</b>	Adenosine Triphosphate
<b>DTT</b>	Dithiothreitol
<b>FAD</b>	Flavin Adenine Dinucleotide
<b>FDP</b>	Flavodiiron Protein
<b>FHP</b>	<i>A. eutrophus</i> Flavohemoglobin
<b>gFIHb</b>	<i>Giardia</i> Flavohemoglobin
<b>Hmp</b>	<i>E. coli</i> Flavohemoglobin
<b>NAD(P)H</b>	Nicotinamide Adenine Dinucleotide (Phosphate)
<b>NOS</b>	Nitric Oxide Synthase
<b>OCT</b>	Carbamoyl Transferase
<b>PMSF</b>	Phenylmethane Sulfonyl Fluoride
<b>rpm</b>	Revolutions Per Minute
<b>SDS-PAGE</b>	Sodium Dodecyl Sulfate Polyacrylamide Gel Electrophoresis
<b>SOD</b>	Superoxide Dismutase
<b>SOR</b>	Superoxide Reductase
<b>Yhb</b>	Yeast Flavohemoglobin



## 1. INTRODUCTION

### 1.1 *Giardia Intestinalis*

The gastrointestinal parasite *Giardia intestinalis* is the causative agent of giardiasis or ‘beaver fever’, a major contributor to diarrheal and intestinal infectious diseases worldwide with over 280 million symptomatic infections annually (1). Diarrheal diseases are collectively the second leading cause of death in children under five years of age in developing countries. Hence, *Giardia* as a main contributor to diarrheal diseases, has a significant impact on global health (2).

The life cycle of *Giardia* alternates between the two forms: cyst and trophozoite. The environmentally resilient and infectious cysts are encapsulated in a tough wall, enabling the parasite to survive outside the host and in the environment. Upon ingestion by a host, the acidic environment in the upper small intestine causes the cysts to differentiate into flagellated binucleated trophozoites through excystation. The trophozoites then reproduce through asexual binary fission. Consequently, infection occurs as trophozoites adhere to the intestinal epithelial cells (IECs) (3). Direct adhesion of trophozoites to IECs induces cellular damage causing malabsorption, maldigestion and electrolyte imbalance, which collectively lead to diarrhea, abdominal cramps and nausea. As trophozoites are swept downstream by peristalsis, new cysts formed through encystation in the lower intestine are then excreted which can contaminate water or, less commonly, food, enabling the parasite to restart its life cycle (4).

*Giardia* is a eukaryote, but it lacks several typical eukaryotic organelles, including peroxisomes, a well-defined Golgi apparatus, smooth endoplasmic reticulum and mitochondria (5). Instead, *Giardia* has mitosomes, which are mitochondrial remnant organelles that retain the ability to assemble iron-sulfur clusters but lack the enzymes for heme biosynthesis. Furthermore, mitosomes are incapable of oxidative phosphorylation, in which the cellular energy currency,

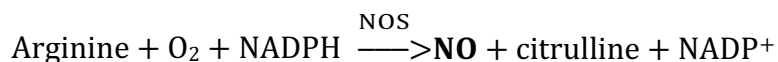
adenosine triphosphate (ATP) is generated from the energy stored in a transmembrane proton gradient. This occurs by movement of electrons through a series of respiratory chain complexes from reduced electron donors (succinate and NADH) to oxygen as the terminal electron acceptor (6). Without this capacity for oxidative phosphorylation, *Giardia* relies on fermentative substrate-level phosphorylation to obtain its required energy which leads to the production of CO<sub>2</sub>, ethanol, acetate and alanine. It also uses pyrophosphate as well as ATP as an energy currency (7). Consequently, *Giardia* is an anaerobic eukaryote in that it does not couple oxygen reduction to ATP synthesis, and it is devoid of catalase, glutathione peroxidase and superoxide dismutase (SOD) which are antioxidant enzymes in most aerobic eukaryotic organisms (7).

*Giardia* is capable of oxygen reduction that is not coupled to ATP synthesis (see below), but this activity at O<sub>2</sub> concentrations above 50 μM does not last more than 90 minutes (8). Since the environment of the upper small intestine infected by *Giardia* is relatively aerobic with O<sub>2</sub> peaking at approximately 60 μM, *Giardia* has to counteract the molecular oxygen in its environment (8). For this purpose, NADH oxidase, flavodiiron protein (FDP), superoxide reductase (SOR) and peroxiredoxins have been identified as the major enzymes involved in the oxidative stress defense mechanism in *Giardia* (9).

Despite lacking mitochondria, and lacking the ability to synthesize heme, *Giardia* encodes at least five heme proteins: four members of the cytochrome *b*<sub>5</sub> family of electron transfer proteins (gCYTB5 isotypes I-IV) and one enzyme of the flavohemoglobin class, gFIHb, that has nitric oxide dioxygenase activity and is thought to counter nitrosative stress (3). The research presented in this thesis investigates the binding of ligands to the heme iron of gFIHb, variants of this enzyme generated by protein engineering, and to its bacterial homolog, Hmp.

## 1.2 Host-Generated Nitric Oxide and its effects on Giardia

In mammals, nitric oxide (NO) is produced from different isotypes of the nitric oxide synthase (NOS) family of enzymes, which use arginine, oxygen, and electrons as substrates:



NO is an important signaling molecule in multicellular organisms, and is especially associated with vasodilation (endothelial NOS) and neurotransmission (neuronal NOS). NO is also produced by mediators of the innate immune system, such as macrophages (inducible NOS), as part of the host antimicrobial defense mechanism (10, 11). In addition to these enzymatic processes, reactive nitrogen species can be generated by the host's diet in the gastrointestinal (GI) tract, particularly upon consumption of nitrite-rich plants such as spinach (12), where the acidic environment of the small intestine favors the reduction of some nitrite to NO (1).

Nitrosative stress caused by reactive nitrogen species such as NO at micromolar concentrations or higher can have detrimental effects on Giardia. NO and its autoxidation products react with and alter the structures and properties of a variety of targets, including the bases of nucleic acids, iron-sulfur clusters (ISCs), tyrosine residues and membrane lipids (13). Aside from these direct impacts, NO generated from neuronal NOS stimulates intestinal motility, which sheds adhered Giardia from the lining of the small intestine (13). Consequently, nitrosative stress has multiple adverse effects on Giardia trophozoites within the host.

Giardia protects itself against nitrosative stress by encoding a flavohemoglobin (gFlHb) which metabolizes the free radical of NO to the less harmful nitrate (3). In addition, Giardia possesses arginine deiminase (ADI) and ornithine carbamoyl transferase (OCT). While Giardia trophozoites use these enzymes to metabolize arginine for energy, they have an additional benefit in depriving

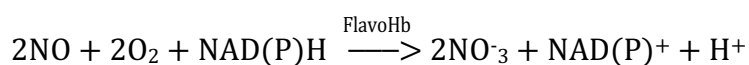
the host's intestinal epithelial cells of a substrate for NOS activity. Furthermore, arginine reduction by OCT and ADI induces apoptosis in IECs (14).

The ability to detoxify NO makes flavohemoglobins important defense mechanisms against nitrosative stress. Indeed, these NO-metabolizing enzymes are up-regulated under nitrosative stress in *Giardia* and *E. coli* (15). Treatment of *Giardia* trophozoites with NO donors such as NONOates results in increased expression of flavohemoglobin (gFIHb) at both the mRNA (ten-fold increase) and protein (five-fold increase) levels (12). This is consistent with increases in the ability of *Giardia* trophozoites to consume NO *in vitro*. In the absence of nitrosative stress, and at a cell density of  $10^6$  cells/mL, *Giardia* trophozoites metabolize NO at the rate of  $0.22 \pm 0.05$   $\mu\text{M}$  NO per minute. However, with prior exposure to  $1$   $\mu\text{M}$  NO, this rate increases threefold (14). Collectively, the NO-dioxygenase activity of gFIHb and the arginine consuming activity of ADI and OCT act in *Giardia* to counter host-generated nitrosative stress, thus allowing the parasite to persist in the host.

### 1.3 Flavohemoglobin Function, Mechanism, and Structure

#### 1.3.1 Function and Structure

Flavohemoglobins are major nitric oxide-metabolizing enzymes that are commonly found in Gram-negative bacteria, and have also been identified in several eukaryotes such as yeast and *Giardia*. These enzymes are nitric oxide dioxygenases, which catalyze the oxidation of the free radical, nitric oxide (NO), to the less harmful nitrate using molecular oxygen and NAD(P)H as cosubstrates (3, 5):



*E. coli* flavohemoglobin (Hmp), with a molecular mass of 44 kDa, was the first flavohemoglobin to be identified in 1991 and has since served as a model for investigations into the physiological role and structural properties of this enzyme class (16). At present, the three-dimensional structure of two bacterial flavohemoglobins (FHP of *Ralstonia eutropha*; Hmp of *Escherichia coli*), and one eukaryotic flavohemoglobin (YHB1 of *Saccharomyces cerevisiae*) have been solved. A homology model of gFIHb (Figure 1) has since been developed based on the characterized structure of Hmp and the relatively high (~ 40%) sequence identity between these two enzymes.

Flavohemoglobins are composed of an amino-terminal globin domain and a carboxy-terminal reductase domain of the ferredoxin nucleotide reductase (FNR) family. The amino-terminal half contains the heme binding globin domain, while the carboxy-terminal half possesses the highly conserved binding sites for electron carriers NAD(P)H and FAD (12, 16). The detoxification of NO occurs via addition of a molecular oxygen ( $O_2$ ), bound at the heme iron which produces nitrate ( $NO_3^-$ ) (17). The globin structure consists of eight alpha helices (A-H) each of which is roughly antiparallel to its neighbors along its amino acid sequence.

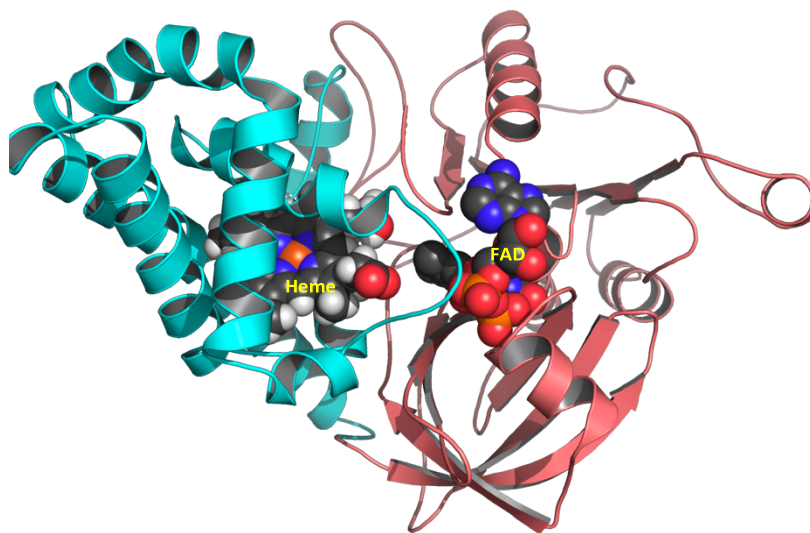


**Figure 1:** Homology model of *Giardia* flavohemoglobin based on the structure of *E. coli* Hmp (1GVH.PDB). The globin domain is highlighted in cyan and the flavin domain is in pink.

### 1.3.2 Active Site Structure of Flavohemoglobin

Heme (Figure 2) is a versatile iron-containing porphyrin cofactor used for a variety of biochemical functions such as oxygen binding and delivery (myoglobin and hemoglobin), redox catalysis (peroxidases, catalase, and hydroxylases) and electron transfer (cytochrome *c* and cytochrome *b<sub>5</sub>*). Heme iron has two common oxidation states: Fe(III), or ferric; and Fe(II), or ferrous. Four of the coordinate bonds to iron in heme proteins are provided by the nitrogen atoms of the porphyrin macrocycle (Figure 2). The protein provides one or two axial ligands to the heme iron, which results in a five-coordinate square pyramidal or a six-coordinate octahedral complex, respectively (12). For instance, O<sub>2</sub>, CO and NO can bind reversibly to the heme iron of flavohemoglobins as exogenous ligands in order to form a Fe(III)-ligand complex.

Heme is a nonpolar cofactor and is found within the interior of the protein, where specific interactions between heme and the surrounding protein environment determine the function of the whole. Such interactions include the coordination between heme iron and axial ligands (e.g. the side chains of histidine, tyrosine, cysteine), van der Waals contacts between heme and adjacent residues, hydrogen bonds within the heme distal pocket between side chains and axial ligands, and, in the case of cytochrome *c*, covalent thioether bonds formed by the reaction of porphyrin vinyl groups and cysteine side chains (12).

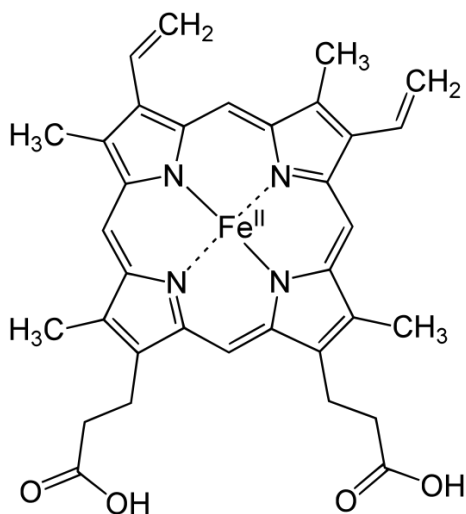


**Figure 2.** The iron containing cofactor, heme, in its reduced (ferrous) state. The four nitrogen atoms of the porphyrin ring act as ligands to the iron; up to two more axial ligands, perpendicular to the plane of the ring, are provided by protein side chains or by the binding of exogenous ligands such as O<sub>2</sub>.

The crystal structures of flavohemoglobins such as bacterial *E. coli* Hmp and eukaryotic *S. cerevisiae* YHB1 have been determined. Based on the alignment of 115 diverse bacterial and eukaryotic flavohemoglobin sequences, several residues surrounding the heme cofactor appear to be invariant in all flavohemoglobins (Figure 3) (18). As is conventional when referring to specific amino acid residues in a globin, one indicates the residue name followed by the helix on which it is found, and its position along the helix. This nomenclature is useful when comparing homologous amino residues from different globins that differ in chain length and hence may have different numbering for the same residue. For example, Tyrosine-30 of gFIHb corresponds to Tyrosine-29 of Hmp, owing to the different chain lengths of these proteins; both correspond to Tyrosine(B10), the tenth residue in their respective B-helices (19).

Heme active site residues in globins are referred to as proximal or distal relative to their position with respect to the plane defined by the heme cofactor. The proximal side refers to the side where the heme axial ligand, Histidine(F8), provided by the protein chain is found, while the distal side is where exogenous ligands such as NO, O<sub>2</sub> or CO bind to the heme iron (Figure 3).

Conserved proximal residues include Histidine(F8), Tyrosine(G1) and Glutamate(H22). While the globin domain of flavohemoglobins share a common protein fold and proximal ligand with the oxygen transporting hemoglobins, O<sub>2</sub> heterolysis is favoured in the former, rather than reversible O<sub>2</sub> binding in the latter. This difference is exerted by differences in the proximal residues, most notably deprotonated Glutamate(H22) that increases the electron density on Histidine (F8) through formation of a hydrogen bond between the carboxylate of the former and the imidazole side chain of the latter. An acidic residue adjacent to the proximal histidine ligand is also observed in the peroxidases, where it promotes O-O bond heterolysis in bound peroxide.

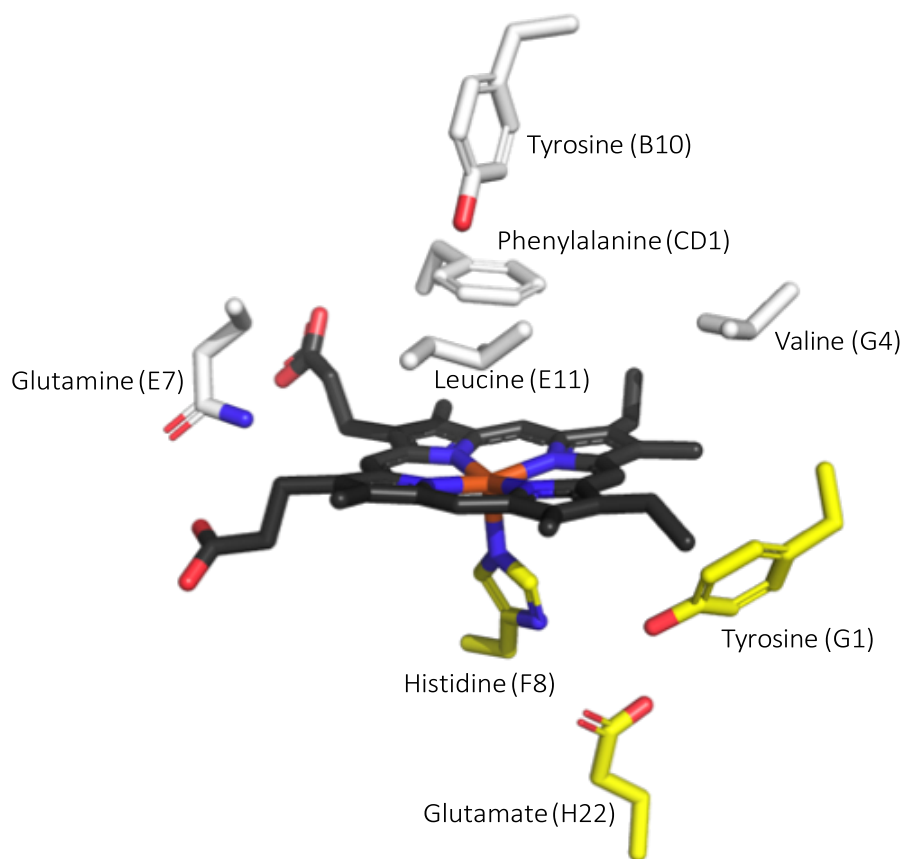


**Figure 3.** Examples of active-site residues conserved in all known flavohemoglobins. The structure is that of *E. coli* Hmp (Protein Data bank file 1gvh.pdb). Black, heme; yellow, conserved proximal residues; white, conserved distal residues.



The properties of the residues in the distal face of the heme – their size, shape, polarity, and hydrogen bonding ability - will affect the affinity of the heme for exogenous ligands. The invariant distal residues of Hmp include both nonpolar and polar residues. Among the former are Phenylalanine(CD1), Leucine(E11), and Valine(G4). Phenylalanine(CD1), which occurs at the corner of the C and D helices is invariant among all known globins, not just flavohemoglobins. It serves an essential structural role in stabilizing heme binding, as its phenyl side chain and the porphyrin ring are coplanar and are in van der Waals contact with each other. Invariant polar residues include Tyrosine(B10), Asparagine (CD2), and Glutamine(E7). Among these, Tyrosine(B10) and Glutamine(E7) are known to stabilize binding of small exogenous ligands bound to the heme iron through hydrogen bond formation (18). Binding of ligands to this site requires a large conformational change as the isobutyl side chain of Leucine(E11) occupies the space where a ligand would bind (19). Consequently, for an exogenous ligand such as CO, O<sub>2</sub> or NO to bind to the heme iron, Leucine(E11) must shift out of this position. This is seen in the structures of flavohemoglobins in different ligation states. For example, when comparing yeast FHP and *E. coli* Hmp, the overlaid structure of these two flavohemoglobins suggests that the position of the E-helix is shifted far from the heme cofactor in FHP in order to accommodate a bulky phospholipid molecule which shifts the positioning of the distal residues (18).

Furthermore, in the CO-bound state Hmp adapts two conformations. The closed conformation is characterized by a hydrogen bonding network between the exogenous bound ligand and surrounding distal residues, while in the open conformation there is no such hydrogen bond network. In the case of Hmp, Tyrosine(B10) interacts with diatomic ligands such as O<sub>2</sub> and CO (20). The transition from open to closed conformation occurs by movement of the NAD-

binding domain associated with a large rearrangement of the C-terminal segment from the FAD binding domain towards the gap where all three domains meet (21).

### *1.3.3 Nitric oxide dioxygenase activity of flavohemoglobins*

In flavohemoglobins, heme plays a crucial role in the course of NO detoxification. Based on the proposed mechanism for the catalytic cycle of flavohemoglobins (Figure 4), the NO-metabolizing process initiates when the ferroheme iron (II) reduces bound O<sub>2</sub> to form superoxide (O<sub>2</sub><sup>-</sup>). Nitrate is then produced as NO reacts with the bound superoxide. After releasing nitrate, ferroheme (reduced state) is then regenerated from the ferriheme iron (III) by a one-electron reduction from the flavin domain, with NAD(P)H as the electron source. However, since NAD(P)H can only donate electrons in pairs, a flavin redox cofactor, FAD, is used to receive electrons from NAD(P)H and donate them singly to the heme iron. This enables the NO-detoxifying cycle to restart (12). An alternative proposed mechanism suggests that NO first binds to the ferroheme iron (II) which is then followed by O<sub>2</sub> addition in order to convert nitric oxide to nitrate (22). The enzyme is inhibited at high concentrations of NO which supports the idea that dioxygenation mechanism in which O<sub>2</sub> binds to the heme iron first is likely to be the accepted mechanism. In addition to the NO-detoxifying role of flavohemoglobins, they may be involved in protecting microorganisms against oxygen, based on their structural and functional properties. In the absence of O<sub>2</sub>, flavohemoglobins reduce nitric oxide to nitrous oxide, N<sub>2</sub>O (17).

Binding of exogenous ligands to gFIHb may represent a pathway to the development of drugs that specifically target the ability of Giardia to counteract nitrosative stress. There are several ways to quantify the binding of a ligand to a heme protein. The simplest relies on spectroscopic changes that occur that are associated with changes in the heme environment as a ligand binds.

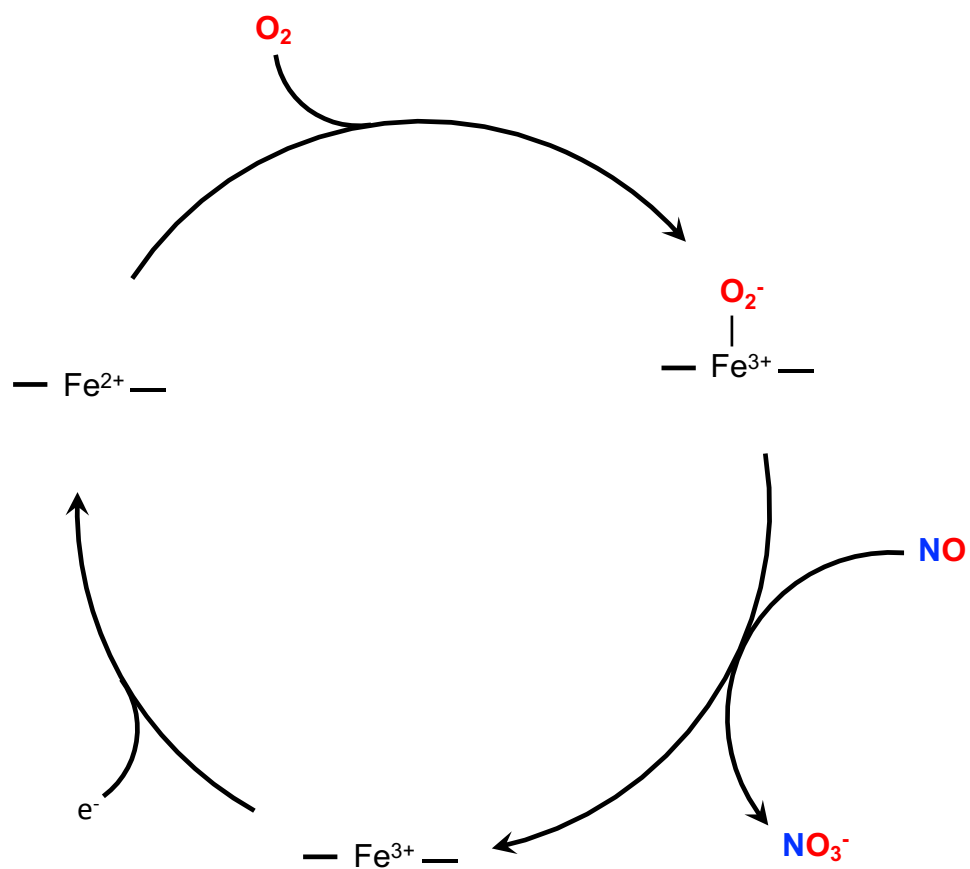


**Figure 4:** The catalytic cycle for NO-dioxygenase activity of flavohemoglobin. Heme is represented as  $\text{—Fe—}$ . The electron that reduces  $\text{Fe}^{3+}$  to  $\text{Fe}^{2+}$  is provided from NAD(P)H *via* the FAD cofactor.

#### 1.4 Characteristics of Giardia Flavohemoglobin (gFlHb)

Giardia is devoid of heme biosynthesis, yet it encodes a flavohemoglobin (gFlHb, Giardia Database ID GL50803\_15009), that, when expressed recombinantly, is obtained with heme and flavin bound and which has nitric oxide dioxygenase activity (3). As Giardia lacks the heme biosynthetic pathway it likely obtains its heme cofactor from its host or the contents of its digestive tract (3), although nothing is yet known about how this may occur. Giardia shares approximately 40% sequence identity with *E. coli* Hmp, suggesting that Giardia likely acquired the gene for its flavohemoglobin through a lateral gene transfer from a Gram-negative bacterium. Indeed, gFlHb has a higher level of sequence similarity to the bacterial Hmp than to the eukaryotic FHP of yeast.

Although it resembles other flavohemoglobins in sequence, domain organization, conservation of active-site residues and cofactor content, gFlHb possesses some unique features. Unlike other flavohemoglobins, gFlHb contains two large sequence insertions, one in the N-terminal globin domain (21 amino acids) and one in the C-terminal FAD-binding domain (29 amino acids). These unique sequence insertions are located on the same face of the enzyme and presumably interact with each other (3). The importance of these insertions is unknown; however, they may impact the rate of electron transfer between globin and flavin domains (12).

Recombinant gFlHb is purified in its ferric state with a mixture of high and low spin states. The Soret band corresponding to the heme cofactor is asymmetrical and detected at 403-405 nm (3). Recombinant gFlHb consumes NO with a turnover number ( $k_{\text{cat}}$ ) of  $116 \pm 10 \text{ s}^{-1}$  and an  $\text{O}_2$  affinity of  $K_m=22\pm7 \text{ }\mu\text{M}$ , which is consistent with the oxygen level present in the proximal side of the small intestine (1).

As noted above, studies on *E. coli* Hmp demonstrate that flavohemoglobins can adapt two different conformations (open and closed) when bound to small exogenous ligands such as carbon monoxide; these conformations are also observed for gFlHb (18, 20). Active site mutants of gFlHb have also been prepared. As the three distal residues of Leucine(E11), Glutamine(E7) and Tyrosine(B10) are conserved among all flavohemoglobins, it can be informative to determine the properties of variants at these positions compared to that of the wild type. For this purpose, the Leucine(E11) which has a bulky isobutyl side chain occupying the distal ligand binding site was mutated to alanine, which possesses a smaller methyl group. This is referred to as the gFlHb L58A mutant. In a similar manner, conservative mutations were made at position E7, where leucine replaced glutamine (gFlHb Q54A), and at position B10, where phenylalanine replaced tyrosine (Y30F); in these cases the mutated side chain retains the size and shape of the wild type residue but lacks its ability to participate in hydrogen bonding that is thought to stabilize the complex of flavohemoglobin with small exogenous ligands. This was confirmed from the results from Resonance Raman (RR) spectroscopy experiments on gFlHb and these mutants, which indicate that the two distal residues of Tyrosine(B10) and Glutamine(E7) have an impact on stabilization of bound exogenous ligands, since the Y30F and Q54L mutants of gFlHb had only a single Fe-CO stretching mode (associated with the open conformation) due to loss of hydrogen bonds, with no evidence for a closed conformation (20). In contrast, mutation of LeuE11 to alanine did not alter the open or closed conformation, suggesting it plays no role in these changes.

The experiments mentioned above used the binding of small exogenous ligands (CO, O<sub>2</sub>) to gFlHb and its variants. This thesis will examine the binding of other small ligands (azide, cyanide) as well as larger ones (substituted imidazoles) (Figure 5). The latter will be especially important to characterize, as ideally one would like to develop a drug that would bind specifically to gFlHb

and no other heme protein; this would not be possible with a small ligand, but may be possible with a larger one that is tailored to complement the distal binding site of gFIHb in shape and noncovalent interactions. To obtain key thermodynamic parameters associated with the binding of such ligands, isothermal calorimetry can be used.

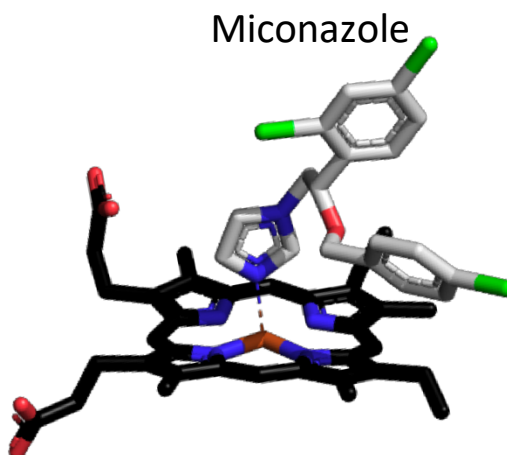


**Figure 5.** Heme active site and miconazole binding to the heme iron with nitrogen atoms shown in blue. Miconazole coordinates to the heme through its imidazole functional group

The heme cofactor is a chromophore with absorption bands in the ultraviolet-visible (UV-Vis) region of the spectrum that are sensitive to its environment, including the binding of ligands to the iron atom of this cofactor. As this thesis makes heavy use of this technique, it is worth briefly describing its theory and its applications.

In UV-Vis spectroscopy, electromagnetic radiation in the ultraviolet or visible regions of the spectrum (approximately 200-800 nm) generates sufficient energy to excite valence electrons, causing them to move from the ground state to a higher energy state which is known as an electronic excitation (23). The energy required to induce excitation can vary due to the strength of chemical bonds and the molecular structures of different compounds. As a result of this

phenomenon, qualitative and quantitative information regarding a particular compound can be obtained by this method of analysis (23).

In heme proteins such as flavohemoglobins, the porphyrin ring causes an intense absorption caused by the transition of an electron from a  $\pi$ -bonding molecular orbital to  $\pi^*$ -antibonding orbital at approximately 400 nm in the UV region; this is known as the Soret band (24). In flavohemoglobins in the oxidized (ferric) state, and in the absence of exogenous ligands, the Soret band is detected at 403-405 nm with a low shoulder between 460-480 nm that corresponds to the flavin associated with the protein (3). Quantitatively, the concentration of the heme proteins can be determined by the application of the Beer-Lambert law by considering the absorbance and extinction coefficient (e.g.  $156,000 \text{ M}^{-1} \text{ cm}^{-1}$  for Hmp as its ferric cyanide adduct) (3, 19). Qualitatively, structural information about the heme active site can be obtained by observing spectral shifts in the Soret band resulting from an exogenous ligand binding to the heme iron (24). UV-Vis spectroscopy can reveal changes in the nature of the heme environment such as oxidation state, spin state, and ligand binding (3, 21). For example, in the flavohemoglobin from the Gram-negative bacteria *Ralstonia eutropha*, UV-Vis spectroscopy indicates that substituted imidazole ligands such as miconazole and econazole bind inside the distal heme pocket and ligate to the iron in the porphyrin ring by their imidazole rings which causes a shift in the Soret band (19). UV-Visible spectroscopy and Soret band of heme proteins can therefore provide valuable information in terms of characteristics of the surrounding residues and ligands in the heme active site. Such changes are the basis for the measurement of dissociation constants for the interaction of ligands with heme proteins by optical titration, in which a series of spectra of a heme protein at different ligand concentrations are recorded.

In ferric flavohemoglobins in the absence of exogenous ligands, the Soret band is detected at approximately 403-407 nm with typical pentacoordinate high spin marker bands in which the proximal fifth ligand is histidine (Figure 6) (19). As an exogenous ligand such as imidazole binds to the flavohemoglobin as its sixth ligand, this causes changes in the wavelengths and absorbances in the spectrum (Figure 6). This information can be used in a plot of ligand concentration  $[L]$  versus absorbance change  $\Delta A$  at a particular wavelength, from which the binding constant of each ligand for the flavohemoglobin can be determined. For a stoichiometry of one ligand binding site per flavohemoglobin molecule, this is done by fitting the data directly to a hyperbolic function to obtain the dissociation constant,  $K_D$ , which is the concentration of ligand required for half of the protein to have ligand bound to it.  $K_D$  has units of concentration, and the lower its numerical value the stronger the binding to the protein. The reciprocal of this value corresponds to the binding constant,  $K_a$ .

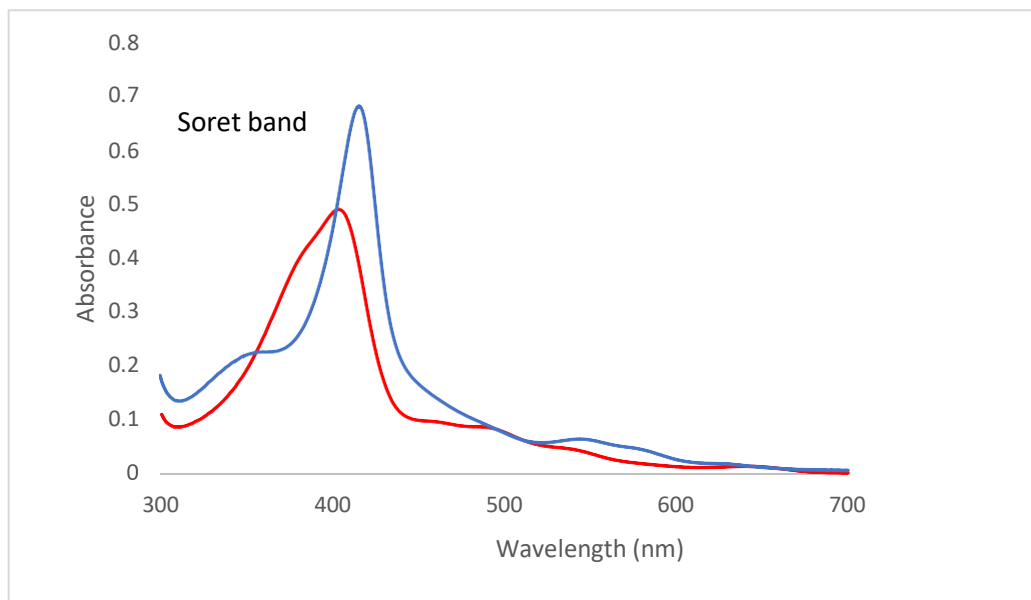


**Figure 6.** Experimental spectroscopic changes in flavohemoglobin on binding of a ligand. Red: ligand-free flavohemoglobin. Blue: imidazole-bound complex



## 1.5 Isothermal Titration Calorimetry (ITC)

Isothermal titration calorimetry (ITC) is a useful technique employed to determine valuable binding information such as the stoichiometry, affinity and enthalpy as a result of a binding interaction between a ligand and a macromolecule such as a protein (25). ITC functions by titrating the ligand into the protein under isothermal conditions which produces a signal corresponding to released or absorbed heat caused by binding of the two participants (25, 26). The thermodynamic parameters are obtained by fitting the experimental data to the isotherm.

In ITC, it is important to use an appropriate range of concentrations for both the ligand and protein to ensure complete titration of the latter (7-25 times more than the concentration of the  $K_D$  for the weakest ligand binding site) (25). ITC uses two cells next to one another: the sample cell contains the protein solution with a syringe provided to inject aliquots of a ligand solution, while the second cell is a reference containing water. With each incremental addition of ligand, heat is released or absorbed in the sample cell due to its binding to the protein. To maintain a constant temperature, the instrument therefore removes or adds heat, with this amount of heat being recorded (Figure 7).

Although it is not as widespread in use as optical titration, ITC offers several advantages over this technique. First, it does not depend on an optical change in the system, and can be used to study protein-ligand interactions in which no optical changes occur. Second, curve-fitting of optical titration data generally relies on the assumption that the free ligand concentration is equal to the total ligand concentration. While this assumption generally holds, it is less accurate in cases of tight ligand binding. In such cases the apparent dissociation constant determined by optical titration will be somewhat higher than the true dissociation constant (that is, optical titration can underestimate the affinity of the protein for the ligand). Third, in addition to the dissociation

constant, further information such as the enthalpy change ( $\Delta H$ ) and entropy change ( $\Delta S$ ) associated with ligand binding can be obtained by ITC as various ligands release (exothermic) or absorb (endothermic) different amounts of heat upon binding to the heme active site of these particular enzymes.

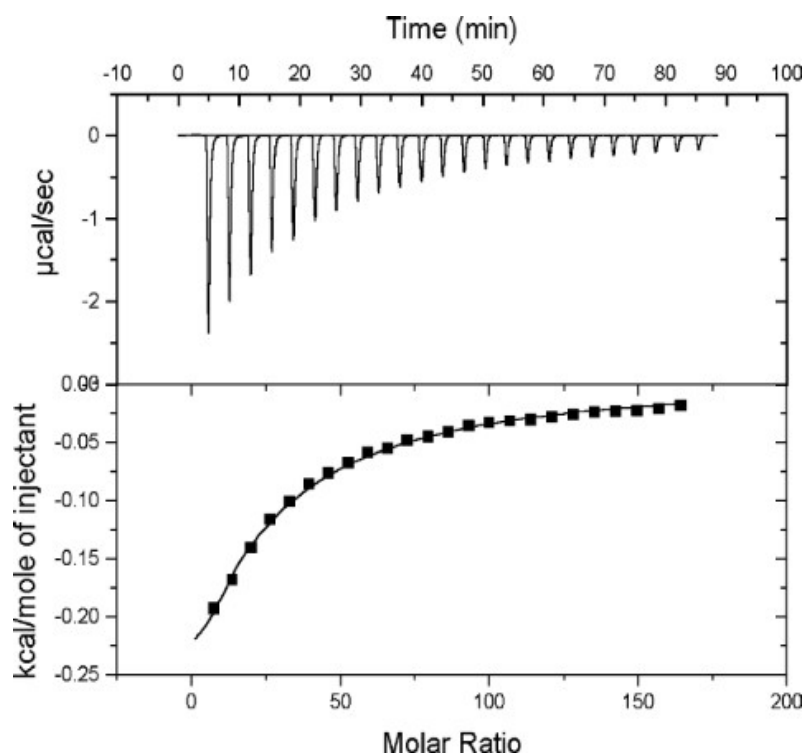


**Figure 7.** One-site model binding isotherm and thermogram obtained by ITC. A representative titration for the exothermic reaction caused by the binding of azide to the heme protein cytochrome *c* peroxidase (27). Upper panel: Raw thermogram corresponding to the binding of azide to cytochrome *c* peroxidase. Lower panel: The one-site model binding isotherm obtained from the integrated thermogram fit.

## 1.6 Thesis Aims

The goal of this research is to determine the ligand binding properties of wild type gFIHb and to compare them to those of *E. coli* Hmp by using optical titration. As gFIHb enables *Giardia* to counter the detrimental effects of NO on the pathogen, it could be a novel pharmacological target. It was previously demonstrated thatazole-based heme-binding ligands, particularly

substituted imidazoles, effectively inhibit the flavohemoglobin NO dioxygenase activity; recent studies have shown that flavohemoglobins can be inhibited by antibiotics with this functional group which acts as a ligand to the heme iron (28). Additionally, the binding of the antibiotic miconazole to the heme iron of *Staphylococcal aureus* flavohemoglobins has been shown to increase the intracellular oxidative stress and enhance the antimicrobial effect against this bacterium (29,30). Consequently, the binding affinities of azide, cyanide and of the imidazole-based ligands (imidazole, 1-methyl imidazole, 1-butylimidazole and miconazole) for gFIHb and three mutants were measured by optical titration. In some cases, the insights into gFIHb binding affinity gained by these experiments were further explored by means of ITC.

The second objective of this research is to determine the impact of the three conserved distal residues Leucine-58(E11), Glutamine-54(E7) and Tyrosine30(B10) on binding of these ligands to gFIHbs. These correspond to residues L58, Q54 and Y30 by numbering of the gFIHb chain. To do this, I will study the three mutants at these positions that we have at hand: L58A, which replaces an isobutyl side chain that blocks the ligand binding site to a methyl group; and the two mutants Q54L and Y30F, both of which lose potential stabilizing H-bonds to the bound ligand.

Finally, when treating Giardiasis, it would be desirable to inhibit the flavohemoglobin of this gastrointestinal parasite while leaving that of a commensal microorganism (*E. coli*) unaffected. Although many distal residues are conserved among flavohemoglobins, it is hypothesized that gFIHb and Hmp may possess different ligand binding properties due to the presence of some different residues at the heme active site (Figure 8) as well as showing approximately 60% diversity in their sequence alignment (Figure 9). The ligand binding studies and comparison of the two flavohemoglobins gFIHb and Hmp may lead to the development of a specific inhibitor for gFIHb which does not affect other non-pathogenic commensal microorganisms such as *E. coli*.



## 2 PROCEDURES

### 2.1 Protein Expression and Purification

#### 2.1.1 Protein Expression

Recombinant protein expression and purification were conducted using the same methods for the wild type and mutant (L58A, Q54L and Y30F) gFlHb enzymes as well as for the *E. coli* Hmp. Initially, pET-14b vectors containing the sequences for either hexahistidine-tagged gFlHb or Hmp, and conferring resistance to ampicillin, were transformed into competent *E. coli* BL21(DE3) cells (New England Biolabs). This was done by adding 1-2  $\mu\text{L}$  containing 50-200 ng of plasmid DNA directly to 50  $\mu\text{L}$  competent cells, thawed and kept on ice, followed by flicking the tube 4-5 times. The mixture was then placed on ice for 30 minutes. Afterwards, cells were heat shocked for 10 seconds at 42 °C and placed on ice for 5 minutes to allow the cells to recover. A 950  $\mu\text{L}$  aliquot of room temperature SOC or LB media was then added to the cell mixture and mixed by gently pipetting up and down. The cell mixture was then transferred into a culture tube and placed in a 37 °C incubator shaker for 60 minutes. Finally, 50  $\mu\text{L}$  of the recovered cells was plated onto an LB agar plate with ampicillin (50  $\mu\text{g}/\mu\text{L}$ ) and incubated overnight at 37 °C.

The next day, a single colony of the plated bacteria was obtained and used to inoculate a 2 mL culture containing Terrific Broth (TB) media with ampicillin (100  $\mu\text{g}/\text{mL}$ ). The culture was then incubated in a shaker at 37 °C for approximately 4-6 hours. Next, the 2 mL culture was used to inoculate 400 mL of TB media containing 100  $\mu\text{g}/\text{mL}$  ampicillin, 3  $\mu\text{M}$  ferric citrate and 100  $\mu\text{M}$  riboflavin in a 2.8 L Fernbach culture flask. The culture was incubated in a shaker covered loosely with tinfoil for approximately 24 hours at 30°C until it reached an optical density (absorbance at 600 nm) of approximately 15. The 400 mL culture was poured into 250 mL

centrifuge tubes and cells were pelleted at 6084 g (6300 rpm) using an SLA 1500 rotor for 15 minutes. Pellets were collected, weighed and frozen at -80 °C.

### 2.1.2 Protein Purification

Frozen pellets were thawed at room temperature and resuspended in 40 mL of binding buffer (50 mM Tris-HCl, 500 mM NaCl, pH 7.5) containing 1% of the detergent, OTG. The resulting cell suspension was vortexed and mixed by pipetting up and down until a homogenous suspension was achieved. Several milligrams of the serine protease inhibitor PMSF were then added to the resuspended cells followed by rocking gently on ice for 10 minutes. The resulting lysate was centrifuged at 12000 g (10000 rpm) using a SS34 rotor for 30 minutes to remove cellular debris. The supernatant was retained, and pellets were discarded.

All flavohemoglobins used in this research were purified in the same manner by taking advantage of the hexahistidine tag on their N-terminus. Initially, a 5 mL column of NiNTA Fast Flow resin (Thermo-Fisher/Pierce, Ottawa ON) was equilibrated by adding 25 mL of binding buffer (50 mM Tris-HCl, 500 mM NaCl, pH 7.5). The supernatant that was obtained after centrifugation of the cell lysate and was loaded onto the column by gravity flow. Following loading, the column was washed with 25 mL of wash buffer (50 mM Tris-HCl, 500 mM NaCl, 25 mM imidazole, pH 7.5). The purified protein was then eluted by adding a minimal volume of the elution buffer (50 mM Tris-HCl, 500 mM NaCl, 250 mM imidazole, pH 7.5) to release the protein from the column by using gravity flow.

Collected protein solutions were concentrated by using Ultra 15 mL Centrifugal Filters with a 30 kDa molecular weight cutoff. Protein samples were added to the ultrafiltration membrane and centrifuged in a swinging bucket SH-3000 rotor at 4200 g for 20 minutes until the protein solution was less than 1 mL in volume. Buffer exchange was also done using the same method

where protein solutions were spun down 3-5 times and after each run, the buffer of interest was added to the sample while the old buffer was eluted.

Residual imidazole from the elution buffer was removed by gel filtration chromatography on a 10 mL Bio-Gel P-6DG column (Bio-Rad, Mississauga ON). The column was equilibrated by adding 50 mL of 20 mM Tris-HCl, pH 7.5. Several milligrams of potassium ferricyanide were added to the purified protein for two purposes: first, to track the position of imidazole and second to oxidize the protein to its ferric state. The resulting protein solution was added to the desalting column. The red band containing desalted protein was collected while the yellow band (ferricyanide and co-eluting imidazole) was discarded.

Protein concentrations were determined by recording their spectra on a Cary 400 Bio UV-visible spectrophotometer. For this purpose, the absorbance of the Soret band (403-405 nm) corresponding to the heme group of the oxidized protein was considered presuming that the extinction coefficients of the wild type and mutants were identical with the numerical value of  $99.1 \text{ mM}^{-1} \text{ cm}^{-1}$  for the ferric, ligand-free complex, or  $156 \text{ mM}^{-1} \text{ cm}^{-1}$  for the ferric cyanide complex (19).

Alternatively, the Bradford assay was employed in order to determine the concentrations of gFlHb and *E. coli* Hmp on a Cary 400 Bio UV-Visible spectrophotometer at 595 nm. For this purpose, a standard curve was obtained by measuring the absorbance values of six 1.2 mL aliquots containing 1 mL Bradford reagent, bovine serum albumin (BSA) at 0, 2, 4, 8, 12 and 16  $\mu\text{g}$  and Millipore water. The  $A_{595}$  of gFlHb and *E. coli* Hmp were measured by diluting the protein 25-fold and substituting them for BSA. The final concentrations were determined by deriving the mass to absorbance correlation of the standard curve by assuming the molecular masses to be 52

and 44 kDa for gFlHb and *E. coli* Hmp, respectively. Each assay was performed in duplicate for accuracy.

The heme content of *E. coli* Hmp and gFlHb was determined using the pyridine hemochrome assay in which heme protein is denatured and heme is released in a basic solution of pyridine. When reduced by sodium dithionite, ferrous heme forms a bis-pyridine complex with characteristic absorption bands at 524 nm and 556 nm. For this purpose, two reagents were prepared: reagent A contained 1 mL of 1 M NaOH, 2.5 mL of pyridine and 1.5 mL of water, while Reagent B was solid sodium dithionite. The Cary 400 Bio UV-Visible spectrophotometer was first zeroed using a 1:1 mixture of 0.5 mL of Reagent A and 0.5 mL of Tris-HCl pH 7.5. The assay comprised of 0.5 mL of Reagent A and 0.5 mL of Tris-HCl pH 7.5 containing the enzyme. The spectrum was recorded between 500 nm and 700 nm. 1-2 milligrams of reagent B were added to the assay, which was mixed gently with a transfer pipette. The heme concentration was determined from the difference in the absorbance at 556 nm and 540 nm using an extinction coefficient of 22.1 mM<sup>-1</sup> cm<sup>-1</sup>. This method was used to complement the results for protein concentrations determined by Bradford assay and UV-Vis measurements on the enzymes.

Recombinant flavohemoglobins were run on 10% SDS-PAGE gels to determine their purity. 3-5 µg of flavohemoglobin mixed with 5 µL of 4x SDS loading dye, containing 0.1 M of freshly-prepared reducing agent dithiothreitol (DTT), and was made up with DI water to a final volume of 20 µL. Samples were heated at 90°C for 5 minutes and centrifuged at maximum speed (typically 13,000 rpm) for 5 minutes using a benchtop centrifuge. Protein samples were separated on a 10% polyacrylamide gel. The resulting gel was stained using Coomassie Blue G-250. Figure 10 depicts the results of separation of each enzyme on 10% SDS-PAGE.



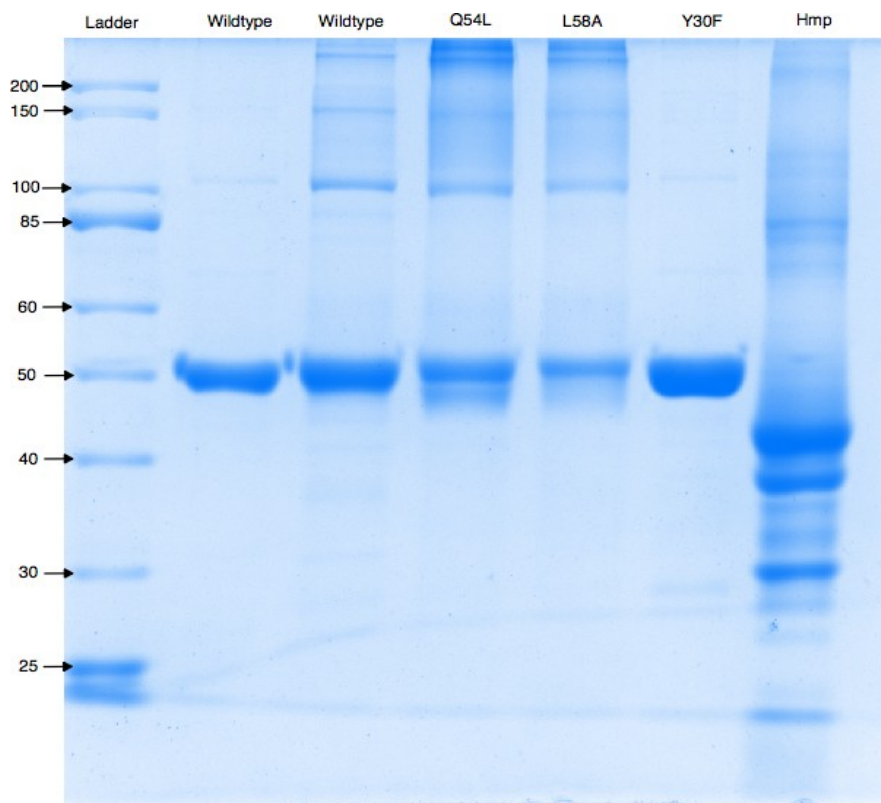


**Figure 10.** 10% SDS-PAGE of purified WT, Q54L, L58A, Y30F and Hmp indicating a molecular weight of approximately 52 kDa for WT, Q54L, L58A and Y30F and 44 kDa for Hmp. From left to right 5  $\mu$ g of gFIHb wild type protein was loaded onto the second lane while the rest of the bands were filled with 7  $\mu$ g of protein samples.

## 2.2 Assessment of Lipid Binding to Flavohemoglobins

*E. coli* Hmp, which is known to associate with phospholipids, was further purified on a microceramic hydroxylapatite resin to remove any residual lipid that might potentially interfere with exogenous ligand binding to the heme iron. Hmp was exchanged into a 5 mM phosphate buffer pH 7.0 by using micro-concentrators as previously described. The protein was then loaded onto a hydroxylapatite column containing 2 mL of the resin equilibrated with the same buffer, and was eluted with 15 mM phosphate buffer pH 7.0 (31).

Lipid extraction was conducted on both WT gFlHb and *E. coli* Hmp using a mixture of chloroform, methanol and DI water in such proportions that a miscible system is formed with the lipid present in the chloroform layer at the bottom while non-lipids were found to be in the methanol-water top layer. For this purpose, 1 mL of concentrated protein (WT gFlHb or Hmp) was used to detect the presence of lipids. To the protein solution, 1 mL of chloroform and 2 mL of methanol was added. The mixture was then vigorously vortexed for 30 seconds followed by addition of another 1 mL of chloroform and 1 mL of DI water. The mixture was again mixed and incubated for 5 mins to obtain distinctly separated layers (32).

The resulting chloroform layer for each protein was then tested on a TLC plate to determine their lipid content. A mixture of *n*-butanol/water/acetic acid (4 : 2 : 1, v/v) was used as the eluent. The resulting TLC plate also contained the two controls of phosphatidylethanolamine (PE) and phosphatidylglycerol (PG) which were observed under the UV lamp and after exposure to iodine vapor (32).

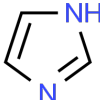
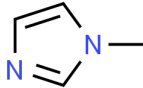
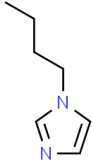
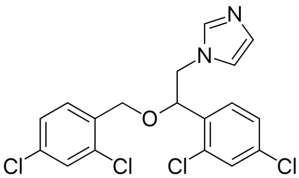
### ***2.3 Optical Titration of Flavohemoglobin with Exogenous Ligands***

A Cary 400 Bio UV-Visible spectrophotometer was used to assess the formation of flavohemoglobin complexes with exogenous ligands (Table 1). Measurements were taken between 250-700 nm using a 3 mL quartz cuvette. The temperature of the cell was maintained at 22°C by means of a temperature controller to prevent any possible effects of temperature on ligand binding properties of the enzymes of interest. Initially, a baseline was obtained by running 20 mM Tris-HCl pH 7.5 buffer which was subtracted from all spectra. A series of experiments were conducted to determine the optimal concentration range for each ligand according to their binding affinities for each enzyme. Nine solutions containing the same concentration of purified flavohemoglobin (3.5  $\mu$ M) with varying concentrations of ligand of interest were prepared for each optical titration, and their spectra were recorded. Optical titrations were performed in duplicates. Wavelengths associated with maximal absorbance differences were used to determine  $\Delta A$  values, which were then plotted against ligand concentration. The data were fit to a hyperbolic function that is expected for 1:1 ligand to protein binding on Mycurvefit.com to analyze spectra and determine  $K_D$  as described above and based on the following equation.

$$\Delta A = \frac{\Delta A_{max} * [L]}{K_D + [L]}$$

Here,  $\Delta A$  is the observed absorbance difference,  $[L]$  is the ligand concentration,  $\Delta A_{max}$  is the maximum absorbance difference when the protein is saturated with ligand, and  $K_D$  is the dissociation constant.

**Table 1.** Properties of the ligands used in this work

Ligand	Formula	Molar mass (g/mol)	Structure
Sodium azide	NaN <sub>3</sub>	65.0	$\text{N}^{\ominus}=\text{N}^{\oplus}=\text{N}^{\ominus} \text{Na}^{\oplus}$
Sodium cyanide	NaCN	49.0	$\text{C}\equiv\text{N}^{\ominus} \text{Na}^{\oplus}$
Imidazole	C <sub>3</sub> H <sub>4</sub> N <sub>2</sub>	68.1	
1-methylimidazole	C <sub>4</sub> H <sub>6</sub> N <sub>2</sub>	82.0	
1-(n-butyl)imidazole	C <sub>7</sub> H <sub>12</sub> N <sub>2</sub>	124.2	
Miconazole	C <sub>18</sub> H <sub>14</sub> Cl <sub>4</sub> N <sub>2</sub> O	416.1	

#### ***2.4 Isothermal Titration Calorimetry (ITC) of Ligand Binding to Flavohemoglobins***

ITC ligand-binding experiments were conducted with a Microcal ITC 200 at the Department of Chemistry, University of Waterloo, Ontario. Samples of gFlHb and Hmp were prepared at Trent University at concentrations of approximately 45-65  $\mu\text{M}$  and kept in a cooler at 4  $^{\circ}\text{C}$  during transport to avoid protein denaturation. Each sample of enzyme and ligand solution was degassed prior to sample run to avoid signal artifacts due to air bubbles during titration, and the exact concentrations of proteins were determined by UV-Visible spectrophotometry on a Cary 1 instrument. Both protein and ligand were dissolved into 20 mM Tris-HCl, pH 7.5 buffer. Methanol and ethanol, the two solvents for 1-(*n*-butyl)imidazole and miconazole respectively, were incompatible with the instrument and therefore these ligands were not used for the ITC experiments.

An instrument calibration was done before each ligand-binding experiment by using the 1:1 binding of  $\text{Ca}^{2+}$  to EDTA. MicroCal ITC<sub>200</sub> Origin software was used to analyze data and simulate binding curves. A control experiment including the titration of the ligand into the buffer solution (20 mM Tris-HCl, pH 7.5) was also conducted to determine the heat of dilution of the ligand which was then subtracted from the obtained thermograms. For the calorimetry studies, instrument parameters were set to the following:

- 40 injections of ligand
- Cell temperature 22  $^{\circ}\text{C}$
- Reference power of 4  $\mu\text{cal}/\text{sec}$
- Initial delay 200 seconds
- Stirring speed 750 rpm

A 100 second interval between injections was used to allow the system to return to thermal equilibrium prior to the next injection. The molar concentration of ligand in the injection syringe was approximately 10-20 times higher than the molar concentration of the protein sample in the

sample cell, as recommended for a 1:1 binding reaction. ITC experiments were done using 0.5  $\mu\text{L}$  of the ligand solution per injection with an initial injection of 0.5  $\mu\text{L}$  to minimize the effect of equilibration artifacts commonly observed with the first injection. Each titration was performed in duplicate.

### 3 RESULTS AND DISCUSSION

#### 3.1 Protein Expression and Purification

Table 2 presents the typical yields of expression of recombinant WT gFIHb and *E. coli* Hmp under the same conditions.

**Table 2.** Recombinant Flavohemoglobin expression yields.

<b>Protein</b>	<b>Cell pellet mass (g)</b>	<b>Flavohemoglobin mass, mg</b>	<b>Yield (mg protein/g cell)</b>
gFIHb	7.52	87	11.6
Hmp	4.48	31	6.9

Based on Table 2, recombinant gFIHb expression yield is higher in comparison with *E. coli* Hmp under the same conditions including expression vector backbone, the type and volume of the media (400 mL TB media), supplemented antibiotic (100 µg/mL of ampicillin) and temperature (30°C). Purified Hmp yielded approximately 6 mg of purified protein from a 400 mL culture based on a previous study which supports the expression yield of Hmp in this work (20). While difficult to rationalize the variation between the expression yields of gFIHb and Hmp, it is speculated that the higher protein expression of WT gFIHb could be due to sensitivity of the two proteins to time and temperature as higher optical density was achieved in Hmp in a shorter time interval (18 hours) while both proteins were left in the incubator shaker for 24 hours before harvesting the cells. Induction of Hmp expression in cells entering the stationary growth phase was also previously detected which is facilitated by RNA polymerase (18). Therefore, Hmp may not have been at its optimal optical density point prior to harvesting the cells at 24 hours. Furthermore, when comparing the results for the purity of the purified proteins by using SDS-PAGE gel, gFIHb and its distal variants indicated high purity with one distinct band while that of Hmp showed several

bands (Figure 10). The presence of multiple bands on the SDS-PAGE gel for the purified Hmp may be due to Hmp being associated with other proteins at lower molecular weights or instability of the purified Hmp.

### 3.2 UV-Visible Spectroscopy

Figure 11 shows the UV-Visible spectra of all four variants of gFIHb and Hmp in their ferric states and in the absence of exogenous ligands. The Soret peaks tend to be asymmetric which is consistent with previous spectroscopic studies on these proteins (20). The spectra of wild type gFIHb and its distal variant L58A are most similar, suggesting that replacement of the bulky isobutyl side chain of leucine does not perturb the heme pockets in this variant. However, both Y30F and Q54L variants of gFIHb have broader and more asymmetric Soret bands at a lower wavelength, associated with a higher fraction of heme in the high spin state. Lukaszewicz previously concluded that Y30F mutant showed broader and more asymmetric Soret band likely due to the slight destabilization of the proximal heme pocket, which confirms the results of this work in this regard (30). In addition, the spectra of variant L58A and Hmp resemble one another in terms of their shapes. Overall, similar spectral characteristics of the wild type gFIHb and its distal variants suggests that the integrity of their heme pockets remain intact (30).



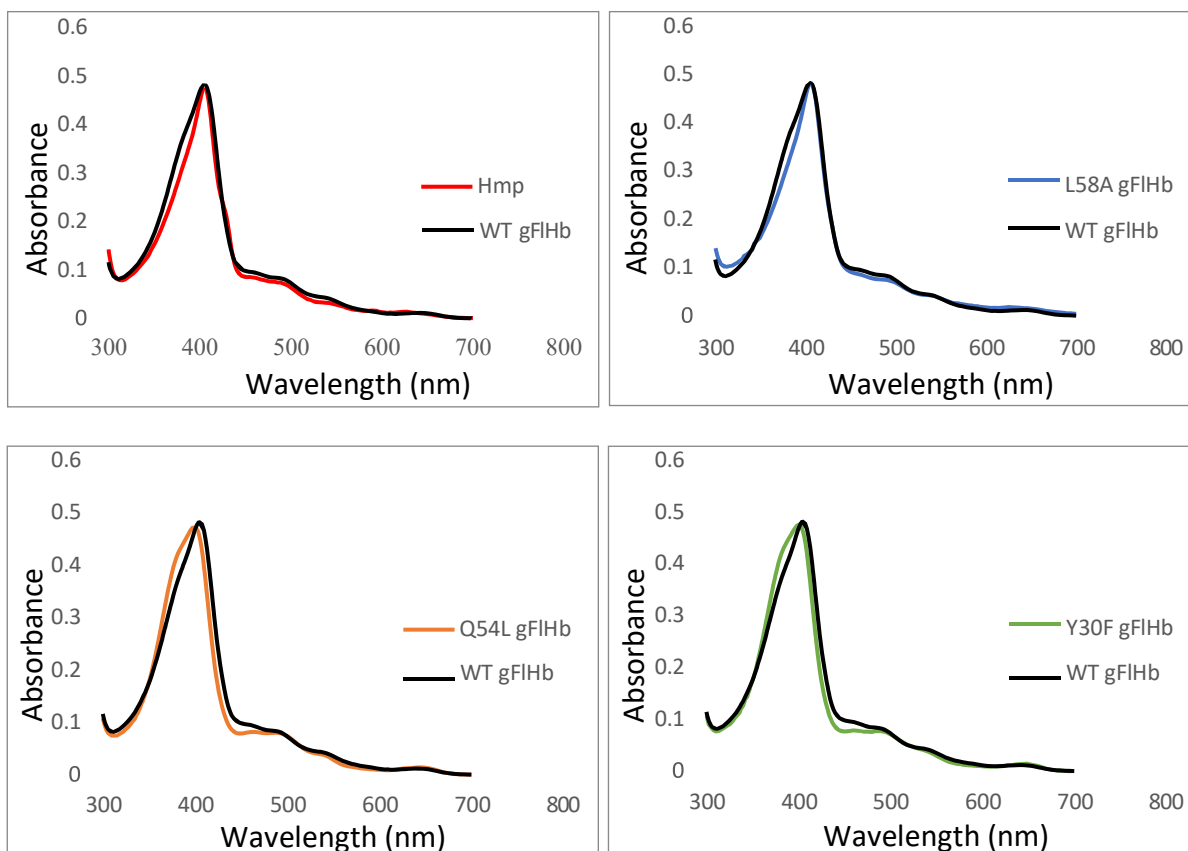


**Figure 11.** UV-Visible spectra of wild type gFIHb, its distal variants of Q54L, L58A, Y30F and *E. coli* Hmp. The protein concentration was 3.5  $\mu$ M and all solutions were in 20 mM Tris- HCl pH 7.5 buffer.

*E. coli* Hmp possesses a more symmetrical Soret band ( $\lambda_{\max} = 401\text{-}403$  nm) while that of wild type gFIHb was determined to be 403-405 nm. These values are consistent with previous reports (19, 20). Furthermore, the more symmetrical Soret band of Hmp suggests that there may be phospholipid bound to the protein at the heme active site (33, 34). Previously, it was discovered that the distal heme pocket of recombinant *E. coli* Hmp is prone to occupation by fatty acids, particularly unsaturated (UFA) and cyclopropanated (CFA) fatty acids. It was proposed that in Hmp, the phosphate head group of the fatty acid is located in an anion-binding cavity adjacent to the heme ring while the double bond or cyclopropane ring of the hydrophobic tail is positioned above the heme iron. Hmp is known to be associated with UFA or CFA as it acts at the interface between the cytosol and the bacterial inner membrane. Based on previous studies, GC-MS

indicated the presence of hexadecanoic acid and *cis*-9,10-methylene hexadecenoic acid in Hmp (19, 20).

As obtained by our purification procedure both gFlHb and Hmp exhibit a Soret band at approximately 403-407 nm and are clearly identified as 5-coordinate high spin species, in which proximal histidine is the fifth ligand. However, based on the work by Illari and coworkers, the spectra of flavohemoglobins with exogenous ligands form 6-coordinate low spin adducts (19, 20).

As Hmp has been reported to be isolated in some cases with phospholipids bound to it, we passed purified recombinant Hmp through a hydroxyapatite column, which has been reported to remove it. Figure 12 depicts the UV-Visible spectra of Hmp before and after passage through hydroxylapatite resin. Our Hmp preparation did not show significant spectroscopic changes with regard to its Soret band after this treatment, which suggests our enzyme was isolated without bound fatty acid.

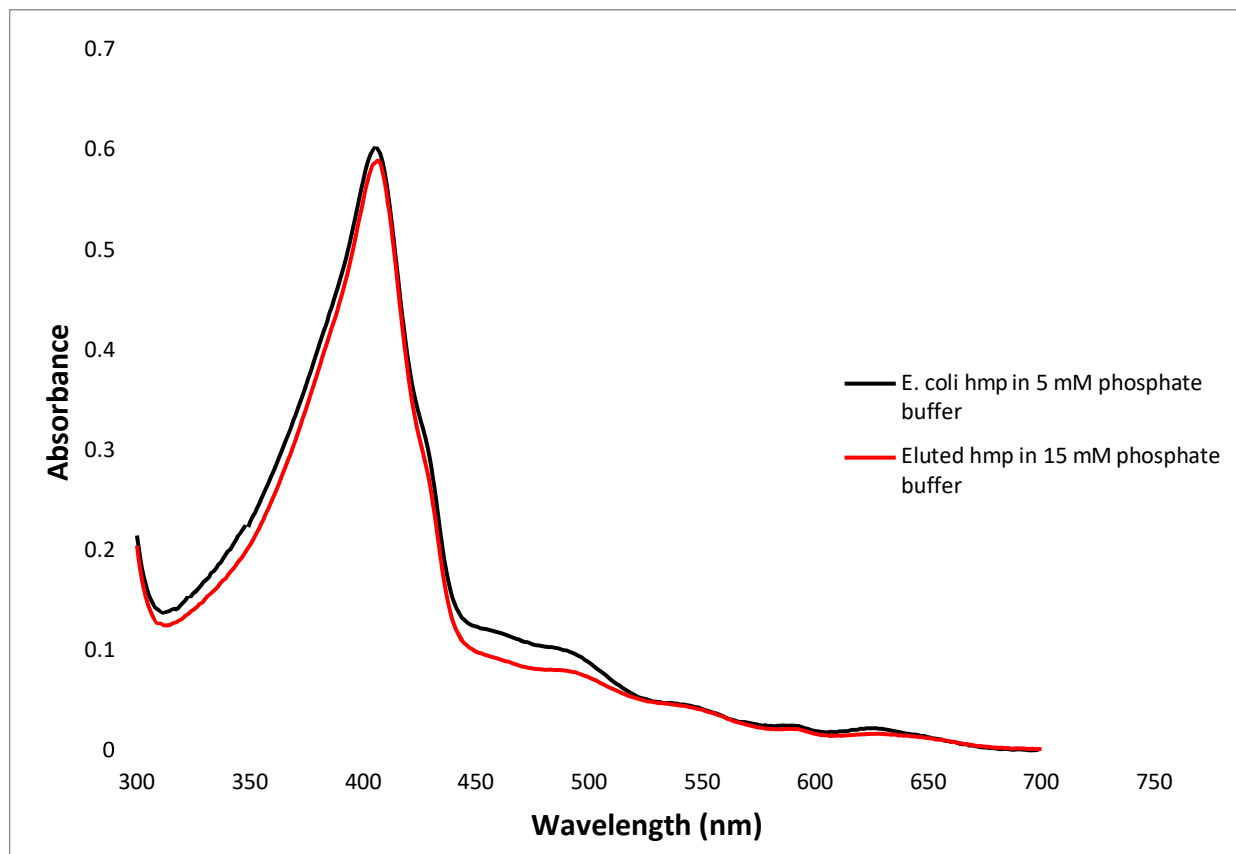


**Figure 12.** UV-Visible spectra of *E. coli* Hmp in phosphate buffer before (in black) and after (in red) running the protein through a microceramic hydroxylapatite column to remove potentially bound phospholipid.

To investigate this further, Hmp and gFlHb were treated with chloroform-methanol lipid extraction followed by TLC to detect whether phospholipids were present in these enzymes (32). As shown in Figure 13, no bands corresponding to the presence of phospholipids were detected in either of our recombinant Hmp or gFlHb enzymes. In contrast, Ollesch and coworkers detected the presence of phospholipids in both Hmp and FHP. There are two plausible explanations for this discrepancy: one is limit of detection by using the TLC method and the other reason could be that there is in fact no phospholipid associated with these two enzymes in our preparations. gFlHb has not been reported to have phospholipids, and our purified Hmp could also be devoid of phospholipids, as the culturing and purification methods were different in this study compared to the study where phospholipid was detected in Hmp. As described in 2.1.2, protein purification was

carried out by using immobilized metal affinity chromatography with a high concentration of imidazole (250 mM) which is a high affinity ligand for the heme iron. It is therefore possible that any phospholipid bound to the heme active site would be displaced by imidazole during NiNTA chromatography. For future experiments, phospholipids can be added back to the purified protein in order to determine how this would impact the ligand binding of the protein of interest.

Phospholipid binding is not a common feature of all flavohemoglobins. *E. coli* Hmp binds the phospholipid between the heme molecule and residues of the globin domain with lower affinity compared to *Ralstonia* FHP, while yeast YHB exhibits no lipid binding (35). Ollesch and coworkers, noted that chromatography on a hydroxylapatite matrix and other softer techniques do not free phospholipids from FHP; instead, they can only be released by denaturing the protein due to the high affinity for lipid binding (35). However, softer techniques are known to release phospholipids from Hmp due to its weaker binding affinity for phospholipids.

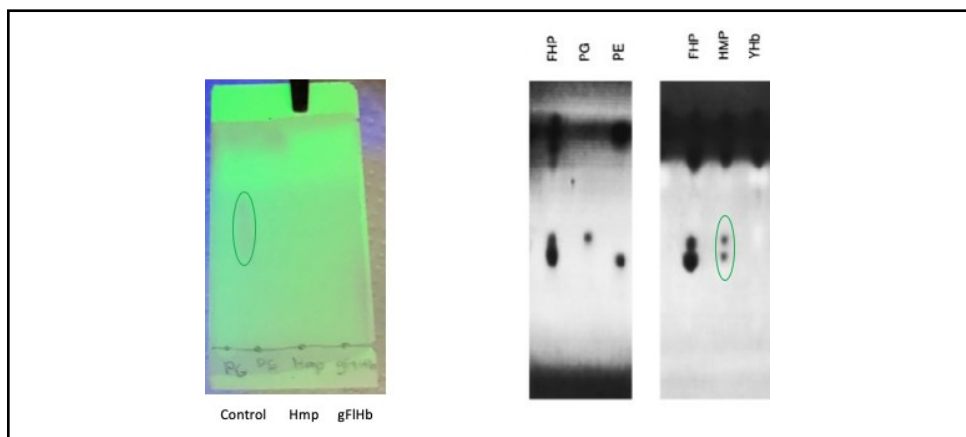


**Figure 13.** Detection of phospholipids in flavohemoglobins. Left, thin layer chromatogram of the lipid extracts from Hmp and gFlHb performed in this work. Right, TLC analysis of FHP (*Ralstonia eutrophus* flavohemoglobin), HMP (*E. coli* flavohemoglobin) and YHB (yeast flavohemoglobin) performed by Ollesch and coworkers (35). Abbreviations: PG, phosphatidylglycerol; PE, phosphatidylethanolamine.

### 3.3 Optical Titration of gFlHb and Variants

Figure 14 presents an example for optical titration and fitted binding curve obtained by the titration of WT gFlHb with 1-(*n*-butyl)imidazole used to calculate  $K_D$ .

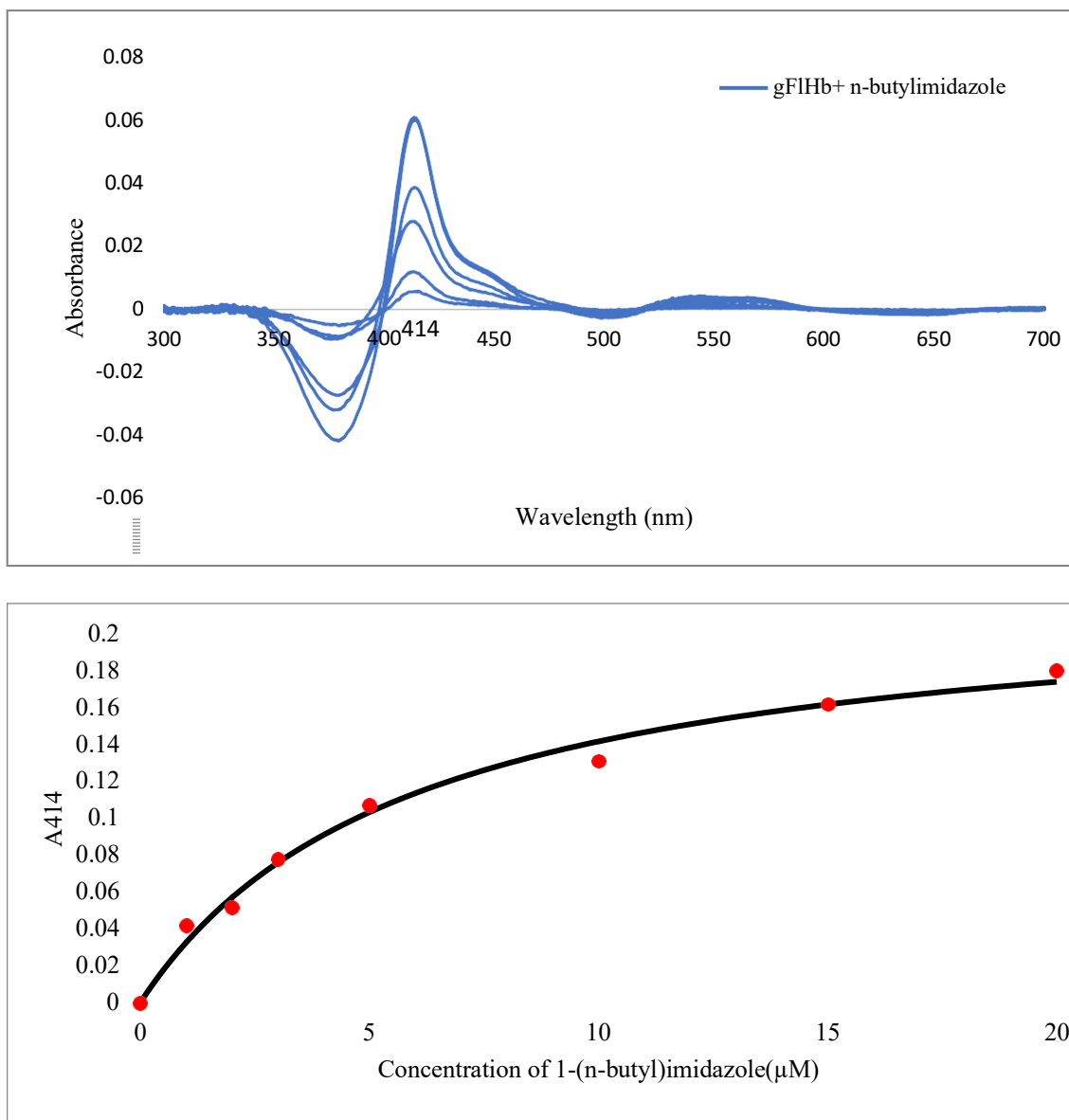


**Figure 14.** Optical titration example with fitted curve as described in section 2.3. **Upper panel:** Spectroscopic changes in absorbance during optical titration of WT gFlHb with 1-(*n*-butyl)imidazole. **Lower panel:** Plot of  $\Delta A$  (difference in absorbance) versus [ligand] with the fitted curve obtained from the optical titration of WT gFlHb with 1-(*n*-butyl)imidazole based on the equation in section 2.3. The protein concentration was 3.5  $\mu\text{M}$  and all solutions were in 20 mM Tris- HCl pH 7.5 buffer.

Table 3 summarizes the dissociation constants of several ligands for the heme iron of wild type gFIHb and the three distal variants Q54L, L58A and Y30F by using optical titrations. Based on Table 3, WT gFIHb has a weak binding affinity for sodium azide, while it possesses relatively strong binding affinities for sodium cyanide as well as imidazole derivatives with the strongest binding affinity for miconazole. The distal variant Q54L binding affinities for the applied ligands are insignificantly different compared to the WT gFIHb. The slight variation for this weaker binding could be explained by considering that Q54 usually hydrogen bonds to the exogenous ligand and is involved in ligand stabilization (19). Thus, removing this hydrogen bond as a result of replacing Q with L may weaken ligand binding since the axial ligand strength is influenced by hydrogen bonds that they may form with surrounding residues (12).

The Y30F mutant of gFIHb, in which phenylalanine replaces tyrosine at the distal site, did not show distinct changes in binding affinity for imidazole and 1-methyl imidazole compared to the wild type enzyme, while the Q54L mutant had weaker binding for both these ligands. This is interesting as both Q54 and Y30 are known to hydrogen bond with small exogenous ligands such as O<sub>2</sub> and CO, and based on these similar roles, their mutants would be expected to have similar binding affinities. A possible explanation for this deviation in their properties could be due to Y30 not having a significant impact on the exogenous ligand binding despite the hydrogen bond loss in the conversion of Tyr to Phe, since Tyr is confined to the second layer of distal pocket residues (19). Another plausible explanation for observing similar binding affinities for the two variants of Q54L and Y30F with the native protein would be that although a hydrogen bond is lost in these mutants, the binding affinity for bulkier ligands such as imidazole substituents is not affected by the loss of this hydrogen bond. Nevertheless, in the case of sodium cyanide which has a high

binding affinity but yet is a smaller ligand, binding affinity is approximately halved between WT gFlHb and its two distal variants of Q54L and Y30F suggesting that loss of hydrogen bond to the exogenous ligand may play a role for stabilization of smaller ligands but not that of larger ligands.

**Table 3.** Dissociation constants ( $K_D$ ) of heme-binding ligands for wild type gFlHb and its distal mutants from optical titrations. Values in parenthesis represent the wavelength at which changes in absorbances were measured.

	$K_D$ , $\mu\text{M}$			
	Wild type gFlHb	L58A	Y30F	Q54L
<b>Sodium azide</b>	1600 $\pm$ 200 (420 nm)	530 $\pm$ 200 (422 nm)	480 $\pm$ 40 (421 nm)	7400 $\pm$ 900 (422 nm)
<b>Sodium cyanide</b>	10 $\pm$ 2 (424 nm)	4 $\pm$ 1 (424 nm)	23 $\pm$ 4 (424 nm)	19 $\pm$ 3 (423 nm)
<b>Imidazole</b>	11 $\pm$ 2 (417 nm)	10 $\pm$ 3 (417 nm)	26 $\pm$ 2 (417 nm)	101 $\pm$ 13 (415 nm)
<b>1-methylimidazole</b>	89 $\pm$ 5 (416 nm)	42 $\pm$ 8 (418 nm)	66 $\pm$ 3 (416 nm)	103 $\pm$ 19 (415 nm)
<b>1-butylimidazole</b>	6 $\pm$ 1 (414 nm)	2 $\pm$ 1 (417 $\mu\text{M}$ )	6 $\pm$ 1 (415 nm)	6 $\pm$ 1 (415 nm)
<b>Miconazole</b>	3 $\pm$ 1 (418 nm)	3 $\pm$ 1 (418 nm)	3 $\pm$ 2 (417nm)	5 $\pm$ 1 (416 nm)

The binding data presented in Table 3 confirms that the affinity of the L58A mutant of gFlHb for exogenous ligands tends to be similar or higher than that of the wild type protein, which may imply that having a smaller residue (alanine versus leucine) at the distal site may facilitate the binding of exogenous ligands to the heme iron. This is reasonable, as ligand binding requires movement of the bulky isobutyl side chain of Leucine-58(E11) away from the bindingsite, which is a large-scale conformational change involving rotation of this side chain as well as rotation and outward shifting of the entire E-helix, as depicted in Figure 15 (18). Presumably such conformational changes are smaller when a smaller residue occupies this position, which will provide greater access for all ligands, as well as more space to accommodate larger ones such as miconazole.

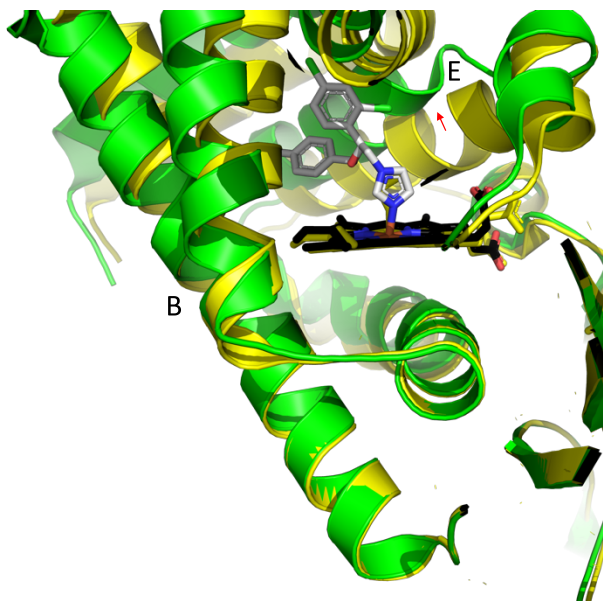


**Figure 15.** Econazole (an imidazole derivative) binding to Yhb showing the movement of E-helix. Yellow, ligand-free heme active site of Yhb (4G1V.PDB). Green, heme active site of Yhb with econazole binding to heme iron (4G1B.PDB).

The dissociation constants of WT gFlHb and *E. coli* Hmp for various ligands were also measured and compared (Table 4). Both gFlHb and Hmp have very low affinities for azide and high affinities for cyanide and substituted imidazole ligands, with miconazole possessing the strongest binding affinity for both flavohemoglobins. Although the binding constants of the two enzymes are slightly different, *E. coli* Hmp and gFlHb result in relatively similar binding affinities for the ligands used in this work, therefore further investigation is required to develop a gFlHb specific inhibitor which does not affect other heme proteins such as *E. coli* Hmp. Nonetheless, the slightly weaker binding affinity observed in Hmp is consistent for all six ligands, with more notable variations observed for sodium azide and sodium cyanide. One plausible explanation for this difference may be due to differences in the amino acid composition within their respective distal sites (Figure 8) and summarized in Table 5. The difference at position E8 is particularly interesting, as proline is considered to be a helix-breaking residue, and it may shorten Helix E by one residue in gFlHb compared to Hmp. The consequences of this difference in a helix known to



undergo a large conformational change in Hmp on ligand binding is in gFlHb unknown, and will have to await direct structural studies on this enzyme in its different ligation states.

It is unlikely that this slight difference in the ligand binding properties of Hmp and gFlHb arise from the presence of phospholipids in Hmp. The results of lipid extraction (Figure 13) along with the purification methods used in this work (2.1.2) would preclude binding composition between lipid and exogenous ligands (35).

**Table 4.** Dissociation constants ( $K_D$ ) for ligand-binding to gFlHb and *E. coli* Hmp. Values in parenthesis represent the wavelength at which changes in absorbances were measured.

	$K_D$ ( $\mu\text{M}$ )	
	<i>Giardia</i> gFlHb	<i>E. coli</i> Hmp
<b>Sodium azide</b>	1600 $\pm$ 200 (420 nm)	26000 $\pm$ 5000 (422 nm)
<b>Sodium cyanide</b>	10 $\pm$ 2 (424 nm)	47 $\pm$ 6 (423 nm)
<b>Imidazole</b>	11 $\pm$ 2 (417 nm)	13 $\pm$ 1 (415 nm)
<b>1-methylimidazole</b>	89 $\pm$ 5 (416 nm)	108 $\pm$ 8 (415 nm)
<b>1-butylimidazole</b>	6 $\pm$ 1 (414 nm)	7 $\pm$ 1 (415 nm)
<b>Miconazole</b>	3 $\pm$ 1 (418 nm)	4 $\pm$ 1 (416 nm)

**Table 5.** Distal site residue differences between gFlHb and Hmp at selected positions

Position	Enzyme	
	gFlHb	Hmp
B14	Leucine	Phenylalanine
CD3	Leucine	Phenylalanine
E12	Leucine	Methionine
E8	Proline	Arginine

### 3.4 Isothermal Titration Calorimetry

ITC was used to obtain information on the thermodynamics of ligand binding. The ITC experiments were conducted on both gFlHb and Hmp with imidazole and 1-methylimidazole (Figure 16). ITC was incompatible with other substituted imidazoles as these were less soluble in aqueous solution. Furthermore, other solvents such as methanol used to dissolve 1-butylimidazole were incompatible with ITC as the solvent addition alone was associated with large heat changes. Figure 16 depicts the raw thermograms subtracted from the buffer-ligand titration (in green) and analyzed data obtained by ITC on imidazole for binding of gFlHb and Hmp.

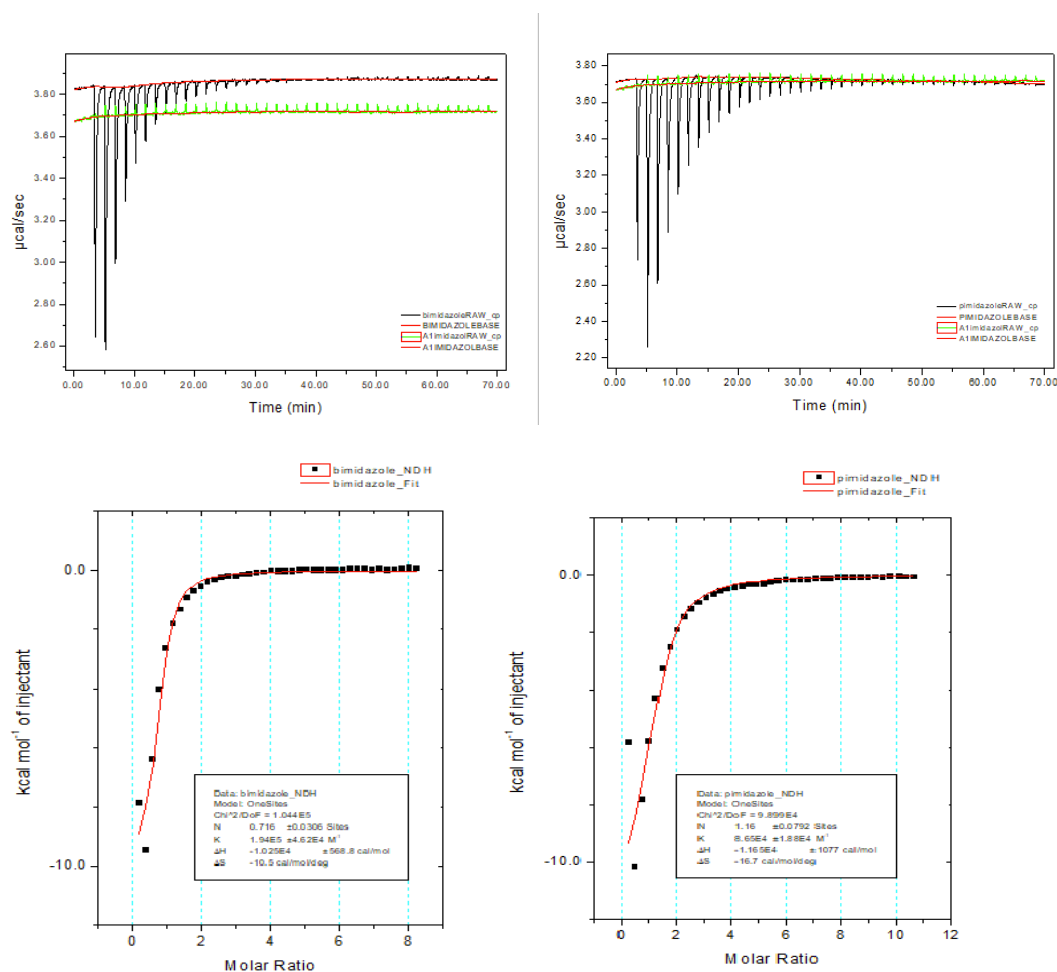


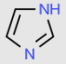
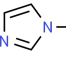
**Figure 16.** Top: Raw thermograms corresponding to the binding of imidazole to gFlHb (left) and *E. coli* Hmp (right). Bottom: The one-site model binding isotherms obtained from the integrated thermogram fit for imidazole binding corresponding to gFlHb (left) and *E. coli* Hmp (right).

ITC determines the binding constants (the reciprocal value of  $K_D$ ) of ligands to receptors which supports the data collected from optical titrations by means of UV-Visible spectroscopy. The ITC titration data are analyzed based on a single binding site as it is expected for flavohemoglobins of both species to have one binding site at the distal site of the heme iron (Figure 7). Based on Table 5, ITC confirms that both enzymes have relatively high binding affinities for imidazole and 1-methylimidazole. Consequently, gFIHb tends to have a stronger affinity for imidazole agents compared to *E. coli* Hmp. This is expected based on the binding constants of these ligands for the two enzymes obtained by means of UV-Visible spectroscopy. ITC results also confirmed slightly weaker binding affinity of Hmp for imidazole derivatives. The possible reasons for this discrepancy in the binding affinity of the two enzymes are discussed in section 3.2.

**Table 6.** Dissociation constants from ITC for ligand binding to flavohemoglobins

	$K_D$ ( $\mu\text{M}$ ), gFIHb	$K_D$ ( $\mu\text{M}$ ), Hmp
<b>Imidazole</b>	$5 \pm 1 \mu\text{M}$	$12 \pm 2 \mu\text{M}$
<b>1-methylimidazole</b>	$30 \pm 5 \mu\text{M}$	$37 \pm 6 \mu\text{M}$

**Table 7.** Thermodynamic parameters from ITC for ligand binding to flavohemoglobins.

Ligand	Enzyme	$\Delta H$ (kcal/mol)	$\Delta S$ (cal/mol/deg)
 <b>Imidazole</b>	<b>gFIHb</b>	$-10.3 \pm 0.6$	-10.5
	<b>Hmp</b>	$-11 \pm 1$	-16.7
 <b>1-Methylimidazole</b>	<b>gFIHb</b>	$-3.7 \pm 0.5$	8.21
	<b>Hmp</b>	$-5.0 \pm .6$	3.43

In addition to  $K_D$ , further thermodynamic parameters such as the binding enthalpy ( $\Delta H$ ) binding entropy ( $\Delta S$ ) and free energy of binding ( $\Delta G$ ) can be determined by ITC. These parameters are related to each other by the equation  $\Delta G = \Delta H - T\Delta S$ . A process such as binding that is favourable as written will have a negative free energy change associated with it.  $\Delta H$  can either be exothermic or endothermic depending on whether heat is released or absorbed, respectively, with a negative enthalpy change favouring the reaction as written. The entropy of a process is a measure of the change in the disorder of a system, or the number of possible microstates of equivalent energy associated with a particular macrostate (25, 26). As a consequence of the second law of thermodynamics, a positive entropy change, corresponding to an increase in the disorder of the system as a result of the process, favors the direction of the reaction as written.

The relationship between  $\Delta H$  and  $\Delta S$  in a ligand-binding reaction is often reciprocal, as the favorable binding enthalpy due to the formation of noncovalent bonds between ligand and receptor is balanced by the entropy loss of translational degrees of freedom as the two molecules combine to form a receptor-ligand complex. However, in large receptors such as proteins, this relationship may be obscured. For example, ligand binding, which is expected to lead to an entropy decrease, may be associated with the release of bound water molecules, which would increase the entropy.

These considerations are seen in in the case of imidazole and 1-methylimidazole binding to the flavohemoglobins gFlHb and Hmp as monitored by ITC (Table 6). The first point to note is that the two flavohemoglobins have similar thermodynamic parameters for binding to each of these ligands. This is expected, based on the similarities in their dissociation constants towards each of these ligands (Table 5). All four ligand-binding reactions have favorable binding enthalpies, with a greater enthalpy change associated with binding of imidazole compared to 1-methylimidazole.

On the other hand, the binding entropies are different, with imidazole binding characterized by a small but unfavourable  $\Delta S$  while that of 1-methylimidazole is favourable.

A possible explanation for these differences in the thermodynamic parameters for the binding of imidazole and 1-methylimidazole might be due to the additional ability of imidazole to act as a hydrogen bond donor, which 1-methylimidazole cannot do. Both molecules can form a coordinate bond between one of their nitrogen atoms and the heme iron, but only imidazole can form an additional hydrogen bond to partners within the heme pocket through its other nitrogen atom. Such a hydrogen bond would be expected to also make the enthalpy of binding more favourable, while at the same time making the entropy of binding less favourable, as formation of a hydrogen bond to a side chain within the heme pocket would require a specific orientation of the ligand. In the case of the flavohemoglobin complex with 1-methylimidazole, the lack of the ligand's ability to form a hydrogen bond may make alternate orientations of the ligand possible due to differences in the angle of rotation about the coordinate bond, which would be manifested as a relatively higher binding entropy.

While a selective inhibitor for gFIHb over *E. coli* Hmp could not be determined in this work, this study provides a basis for further studies to find a more effective antibiotic with less adverse effects to expel *Giardia* from its host's body more effectively. Miconazole demonstrated the strongest binding affinity for both enzymes in this experiment and has previously been shown to inhibit bacterial flavohemoglobin activity. It is worth noting that hydrophobic antibiotics such as miconazole possess poor cell membrane permeability in Gram-negative bacteria such as *E. coli* which contributes to the more evident inhibition of flavohemoglobins in purified enzymes than in intact *E. coli*. A combination of the NO donor compound DETA-NONOate and miconazole exhibited growth inhibition in *E. coli* in which the Hmp gene had been deleted (29). In addition,

miconazole is known to interfere with synthesis of fungal and bacterial lipid membranes as it prevents ergosterol biosynthesis (16, 29). Interestingly, miconazole acts by binding as an axial ligand to a cytochrome P450 monooxygenase that is a member of the ergosterol biosynthetic pathway and is also a heme protein similar to flavohemoglobin.

The crystal structure of the complex of FHP and miconazole shows that its imidazole ring ligates to the heme iron, while the additional substituents, mostly chlorinated phenyl groups, form a series of van der Waals interactions with the protein environment. The combination of both interactions likely explains the high affinity of such substituted imidazoles for flavohemoglobins in general (38). It is expected that this phenomenon also occurs on binding of such compounds to gFIHb, its three distal mutants and Hmp.

Based on research conducted by Gardner and colleagues, *E. coli* Hmp demonstrates dissociation constants of 0.28  $\mu\text{M}$  and 90  $\mu\text{M}$  for NO and O<sub>2</sub>, respectively, which when compared to the results obtained in this study exhibits a significantly stronger binding affinity for the heme iron compared to the imidazole derivatives implemented in this research (39). An improved version of an antiangiogenic drug therefore would need to outcompete both O<sub>2</sub> and NO in order to act as an effective inhibitor for the flavohemoglobin of the pathogenic microorganism.

A study probing the interaction between azole-based antibiotics and *Staphylococcus aureus* flavohemoglobin found that miconazole, the most effective azole-based antibiotic tested binds to the heme iron of both reduced and oxidized states of this enzyme. The dissociation constant of this interaction was reported to be 0.59  $\mu\text{M}$ , supporting a tight and specific binding equilibrium which leads to increased superoxide generation by the enzyme (22, 29). This signifies that imidazole binding to the heme active site of flavohemoglobins including gFIHb and Hmp not only impedes the binding of NO but also increases the intracellular oxidative stress.

### 3.5 Future Directions

This research studied the affinity of flavohemoglobins towards various ligands that could act as enzyme inhibitors. To follow up this work one could determine the affinity of other bulkier imidazoles for gFIHb and *E. coli* Hmp such as econazole. Furthermore, an interesting continuation to this research would be to mutate the three conserved residues of Q53, L57 and Y29 in Hmp to L, A and F, respectively and determine their binding affinities for imidazole agents such as miconazole. This research could confirm the impact of these distal residues on the stabilization of bound exogenous ligands to the heme iron in *E. coli* Hmp. Third, inhibition constants for ligands that show different binding affinities between gFIHb and Hmp could be determined by means of free radical analyzer. This work is currently in progress. Lastly, addition of phospholipid to Hmp followed by determination of the binding affinity of various ligands for Hmp can also be an interesting research topic as Hmp *in vivo* may be associated with phospholipids when imidazole is not used during its purification steps, which may impact the ligand binding affinity of this protein. As for flavohemoglobin inhibition, although results did not determine a specific ligand for gFIHb, inhibition of flavohemoglobins in *E. coli* can also be beneficial as it might enable us to combat other human infections such as a urinary tract infection caused by pathogenic *E. coli* strains (16).

### 3.6 Conclusions

Probing the ligand binding properties of gFlHb, its distal mutants and Hmp by means of optical titrations and ITC revealed important information regarding the connection between the presence of different residues at the heme active site and flavohemoglobins' heme-ligand affinities for various nitrogen containing ligands, particularly imidazole derivatives. Comparative results of ligand binding experiments between the wild type gFlHb, Q54L and Y30F mutants implied that by removing the hydrogen bond between Q54 or Y30 and the exogenous ligand, the heme-ligand binding affinity did not change significantly in particular for bulky imidazole derivatives. Also, when L58, which is known to be the closest distal residue to the heme iron, was replaced with a less bulky alanine residue, the binding affinity improved. This suggests that having a less bulky residue may facilitate access to the heme iron and that having a bulkier ligand such as imidazole derivatives may cause larger rearrangements by shifting the E-helix outwards in order to provide more space for the exogenous ligand.

Optical titration and ITC both indicated slightly stronger heme-ligand binding affinities in gFlHb compared to Hmp, which can be rationalized by the presence of different distal residues at the heme active site of these two flavohemoglobins which may impede the access of the heme iron in Hmp. Nevertheless, as binding affinities in gFlHb and Hmp were similar, we can conclude that the ligands tested in this study cannot act as specific inhibitors for gFlHb.



## REFERENCES

1. Mastronicola, D., Falabella, M., Forte, E., Testa, F., Sarti, P., & Giuffrè, A. (2016). Antioxidant defence systems in the protozoan pathogen *Giardia intestinalis*. *Molecular & Biochemical Parasitology*, 206(1/2), 56–66.
2. Ansell, B. R. E., McConville, M. J., Ma'ayeh, S. Y., Dagley, M. J., Gasser, R. B., Svärd, S. G., & Jex, A. R. (2015). Drug resistance in *Giardia duodenalis*. *Biotechnology Advances*, 33(6), 888–901.
3. Rafferty, S, Luu, B., March, R.E, and Yee, J.. (2010). “*Giardia Lamblia* Encodes a Functional Flavohemoglobin.” *Biochemical & Biophysical Research Communications* 399 (3): 347–51.
4. Carranza, P. G., & Lujan, H. D. (2010). New insights regarding the biology of *Giardia lamblia*. *Microbes & Infection*, 12(1), 71–80.
5. Ma, ayeh, S. Y., Liu, J., Peirasmaki, D., Hörnaeus, K., Bergström Lind, S., Grabherr, M., Svärd, S. G. (2017). Characterization of the *Giardia intestinalis* secretome during interaction with human intestinal epithelial cells: The impact on host cells. *PLoS Neglected Tropical Diseases*, 11(12), 1–41.
6. Tovar, J., León-Avila, O., Sánchez, L. B., Sutak, R., Tachezy, J., Van Der Giezen, M., ... Lucocq, J. M. (2003). Mitochondrial remnant organelles of *Giardia* function in iron-sulphur protein maturation. *Nature*, 426(6963), 172–176.
7. Brown, D. M., Upcroft, J. A., Edwards, M. R. & Upcroft, P. (1998). Anaerobic bacterial metabolism in the ancient eukaryote *Giardia duodenalis*. *International Journal for Parasitology*, (28) 149-164.
8. Raj, D., Ghosh, E., Mukherjee, A. K., Nozaki, T., & Ganguly, S. (2014). Differential gene expression in *Giardia lamblia* under oxidative stress: Significance in eukaryotic evolution. *Gene*, 535(2), 131-139.
9. Mastronicola, D., Giuffrè, A., Testa, F., Mura, A., Forte, E., Bordi, E., & ... Sarti, P. (2011). *Giardia intestinalis* escapes oxidative stress by colonizing the small intestine: A molecular hypothesis. *IUBMB Life*, 63(1), 21-25.
10. Parham, P. (2015). The immune system. New York: *Garland Science*. New York. 4<sup>th</sup> edition.

11. Mastronicola, D., Testa, F., Forte, E., Arese, M., Bordi, E., Pucillo, L. P., & ... Giuffrè, A. (2012). How does the human parasite *Giardia intestinalis* cope with nitrosative stress? *Nitric Oxide*, 27(s1), S46.
12. Rafferty, S. P., & Dayer, G. (2015). Heme proteins of *Giardia intestinalis*. *Experimental Parasitology*, 159, 13-23.
13. Mastronicola, D., Testa, F., Forte, E., Bordi, E., Pucillo, L. P., Sarti, P., & Giuffrè, A. (2010). Flavohemoglobin and nitric oxide detoxification in the human protozoan parasite *Giardia intestinalis*. *Biochemical & Biophysical Research Communications*, 399(4), 654-658.
14. Ringqvist, E., Palm, J. D., Skarin, H., Hehl, A. B., Weiland, M., Davids, B. J., & ... Svärd, S. G. (2008). Release of metabolic enzymes by *Giardia* in response to interaction with intestinal epithelial cells. *Molecular & Biochemical Parasitology*, 159(2), 85-91.
15. Gardner P. (2005). Nitric oxide dioxygenase function and mechanism of flavohemoglobin, hemoglobin, myoglobin and their associated reductases. *Journal of Inorganic Biochem.* 99(1):247-66
16. Svensson, L., Poljakovic, M., Säve, S., Gilberthorpe, N., Schön, T., Strid, S., & ... Persson, K. (2010). Role of flavohemoglobin in combating nitrosative stress in uropathogenic *Escherichia coli* – Implications for urinary tract infection. *Microbial Pathogenesis*, 49(3), 59-66.
17. Lin, Y. (2018). Structure and function of heme proteins regulated by diverse post-translational modifications. *Archives Of Biochemistry & Biophysics*, 64, 11-30.
18. Bonamore, A., & Boffi, A. (2008). Flavohemoglobin: Structure and reactivity. *IUBMB Life*, 60(1), 19-28.
19. Illari, A., Bonamore, A., Faria, A., Johnson, K. & Boffi, A. (2002). The X-ray Structure of Ferric *Escherichia coli* Flavohemoglobin Reveals an Unexpected Geometry of the Distal Heme. *Journal of Biological Chemistry*, 277(26), 23725-23732.
20. Lukaszewicz, B., McColl, E., Yee, J., Rafferty, S., & Couture, M. (2017). Resonance Raman studies on the flavohemoglobin of the protist *Giardia intestinalis*: evidence of a type I/II-peroxidase-like heme environment and roles of the active site distal residues. *Journal of Biological Inorganic Chemistry*, 22(7), 1099-1108.
21. Bonamore, A., Gentili, P., Illari, A., Schininà, M. E., & Boffi, A. (2003). *Escherichia coli* Flavohemoglobin Is an Efficient Alkylhydroperoxide Reductase. *Journal of Biological Chemistry*, 278(25), 22272.

22. Hausladen, A., Gow, A., & Stamler, J. S. (2001). Flavohemoglobin denitrosylase catalyzes the reaction of the nitroxyl equivalent with molecular... *Proceedings of the National Academy of Sciences of the United States of America*, 98(18), 10108.
23. Robinson, J. W., Skelly Frame, E. M. & Frame II, G. M. (2004) *Undergraduate Instrumental Analysis*.
24. Rimington, C. (1960). Spectral-absorption coefficients of some porphyrins in the Soret-band region. *Biochem. J.* 75, 620–623.
25. Duff, M. R., Grubbs, J. & Howell, E. E. (2011). Isothermal Titration Calorimetry for Measuring Macromolecule-Ligand Affinity. *Journal of Visualized Experiments*. (55).
26. Pethica, B. A. (2015) Misuse of thermodynamics in the interpretation of isothermal titration calorimetry data for ligand binding to proteins. *Analytical Biochemistry*, 472, 21-29.
27. Jacobson, T., Williamson, J., Wasilewski, A., Felesik, J., Vitello, L. B., & Erman, J. E. (2004). Azide binding to yeast cytochrome c peroxidase and horse metmyoglobin: comparative thermodynamic investigation using isothermal titration calorimetry. *Archives of Biochemistry & Biophysics*, 422(2), 125.
28. El Hammi, E., Warkentin, E., Demmer, U., Marzouki, N. M., Ermler, U., & Baciou, L. (2012). Active site analysis of yeast flavohemoglobin based on its structure with a small ligand or econazole. *FEBS Journal*, 279(24), 4565–4575.
29. Bang, C. S., Kinnunen, A., Karlsson, M., Önnberg, A., Söderquist, B., & Persson, K. (2014). The antibacterial effect of nitric oxide against ESBL-producing uropathogenic *E. coli* is improved by combination with miconazole and polymyxin B nanapeptide. *BMC Microbiology*, 14(1), 1-9.
30. Nobre, L. S., Todorovic, S., Tavares, A. F. N., Oldfield, E., Hildebrandt, P., Teixeira, M., & Saraiva, L. M. (2010). Binding of Azole Antibiotics to *Staphylococcus aureus* Flavohemoglobin Increases Intracellular Oxidative Stress. *Journal of Bacteriology*, 192(6), 18.
31. Bonamore, A., Chiancone E., & Boffi A. (2001). The distal heme pocket of *Escherichia coli* flavohemoglobin probed by infrared spectroscopy. *Biochimica et Biophysica Acta*. 174-178.
32. Bligh, E.G. & Dyer W. J. (1959). A Rapid Method of Total Lipid Extraction and Purification. *Canadian Journal of Biochemistry and Physiology*. (37).

33. Oellerich, S., Lecomte, Paternostre, M., Heimburg, P. (2004). Peripheral and Integral Binding of Cytochrome c to phospholipids Vesicles. *Journal of Physical Chemistry*, 108(12), 3871-3878.
34. Tuominene, K. J., Wallace, J. A., & Kinnunen K. J. (2002). Phospholipid-Cytochrome c Interaction. *The Journal of Biological Chemistry*. (277), 8822-8823.
35. Ollesch, G., Kaunzinger, A., Juchelka, D., Schubert-Zsilavecz, M. & Ermler, U. (1999). Phospholipid bound to the flavohemoprotein from *Alcaligenes eutrophus*. *Eur. Journal of Biochemistry*. 262, 396-405.
36. Ferreiro, D. N., Boechi, L., Estrin, D. A., & Martí, M. A. (2013). The key role of water in the dioxygenase function of *Escherichia coli* flavohemoglobin. *Journal of Inorganic Biochemistry*, 119, 75–84.
37. Markova, N. (2017). Using Microcalorimetry to Accelerate Drug Development. *Pharmaceutical Technology*, 41(1), 57–59.
38. El Hammi, E., Warkentin, E., Demmer, U., Limam, F., Marzouki, N. M., Ermler, U., & Baciou, L. (2011). Structure of *Ralstonia eutropha* Flavohemoglobin in Complex with Three Antibiotic Azole Compounds. *Biochemistry*, 50(7), 1255–1264
39. Gardner, A., Martin, L. & Gardner, P. (2000). Steady-state and transient kinetics of *Escherichia coli* nitric-oxide dioxygenase (flavohemoglobin). *Journal of Biology & Chemistry*. (275), 12581-12589.